PHILOSOPHICAL TRANSACTIONS OF THE ROYAL SOCIETY A MATHEMATICAL, PHYSICAL & ENGINEERING SCIENCES

High-Frequency Vibration and Acoustic Radiation of Fluid-Loaded Plates

W. R. Graham

Phil. Trans. R. Soc. Lond. A 1995 **352**, 1-43
doi: 10.1098/rsta.1995.0057

High-frequency vibration and acoustic radiation of fluid-loaded plates

By W. R. Graham

Cambridge University Engineering Department, Trumpington Street, Cambridge CB2 1PZ, UK

Contents

Phil. Trans. R. Soc. Lond. A (1995) **352**, 1–43
Printed in Great Britain

To investigate the high-frequency vibration and acoustic radiation of fluid-loaded structures, the model problem of a simply-supported plate excited by a random pressure field is considered. The analysis is standard and yields a set of modal equations coupled by acoustic interaction terms. These terms not only complicate the equations, but also appear in a form that is difficult to evaluate numerically at high frequencies and mode numbers. The latter problem is resolved by deriving asymptotic expressions for the acoustic coefficients, and computational solution of the full, coupled modal equations then becomes feasible. By comparing the results with the 'diagonal approximation' (the solution when coupling is ignored), an improved characterization of the physical nature of the acoustic coupling is obtained, and new conditions for its neglect are specified. The conditions are not stringent, implying that the diagonal approximation will often be valid, and raising the possibility of applying statistical energy analysis (SEA) to significantly fluid-loaded structures. Modified SEA results are derived, and found to compare well with the modal solutions.

1. Introduction

The excitation of a fluid-loaded structure by some form of random forcing is an important problem in many areas of engineering. The presence of the fluid is clearly fundamental to the radiated acoustic field, but it may also affect the structural vibration via the induced acoustic pressures. If the fluid-loading is very light, structural properties always dominate the response, and the solution *in vacuo* for the vibration applies. For somewhat heavier fluid-loading, the presence of the (unbounded) fluid may be accounted for by including additional modal damping and mass terms, but this approximation eventually breaks down, and the exact solution for the combined structural–acoustic vibration must be found. Here the acoustic field in the fluid couples the structural modes *in vacuo*, and the modal equations take a matrix form, with an inevitable increase in complexity. This paper investigates the problem in this region, with the aim of obtaining an understanding of the physical nature of the modal coupling and its effects, and thereby specifying conditions under which approximate solutions become valid.

The specific example considered is the excitation of a flat, fluid-loaded plate by a random pressure field. Such a problem has been analysed many times, either with the coupling terms neglected (see, for example, Davies 1971*a*; Heron 1977) or retained (Davies 1971*b*; Mkhitarov 1972; Sandman 1975; Lomas & Hayek 1977; Leppington *et al.* 1986; Bano *et al.* 1992). Of the latter group of authors, all but Lomas & Hayek compare solutions obtained with and without modal coupling effects accounted for. Sandman's results, for a water-loaded composite plate, show significant differences between the two solutions, as do those of Davies and Bano *et al.*, also for water-loaded plates at low frequencies. On the other hand, Leppington *et al.*, considering the high-frequency, light fluid-loading case, predict that, even if coupling is important, its frequency-averaged effect is nil. Mkhitarov distinguishes between two possible situations, the first where resonant modes do not overlap, in which case a negligible effect is expected, and the second where there is overlap, and coupling is potentially significant.

As a result of this work, some characterization of the coupling has emerged. However, a full understanding of its physical behaviour and a simple set of

PHILOSOPHICAL TRANSACTIONS OF THE ROYAL SOCIETY A MATHEMATICAL, PHYSICAL & ENGINEERING SCIENCES

requirements for its neglect are lacking. Here we address the deficiency by calculating the full solution to the coupled modal equations, and comparing it with that obtained when coupling is neglected. For situations involving many modes, the numerical generation of the modal equations is computationally arduous, and this difficulty is removed by obtaining accurate asymptotic approximations to the coupling terms, valid in the high-frequency limit. The generation of the full solution for the high-frequency region is then feasible.

It is found that the differences between the solutions may be qualitatively explained by using a simple analytical model, with a resulting improvement in the physical characterization of the coupling behaviour. The model is also used to provide simple and general conditions for the neglect of modal coupling, applicable to situations both with and without overlapping resonances. The requirements are likely to be satisfied in most practical cases, suggesting that further approximations, following the methods of statistical energy analysis (SEA), may also be valid. SEA expressions for the power radiated by the plate exist for the light fluid-loading problem (Davies 1971*a*; Heron 1977; Leppington *et al.* 1986), but these require modification for the heavy fluid-loading case. New formulae are therefore obtained and compared with the modal solutions for plate radiation.

The paper consists of three main sections. In §2, the fundamental analysis for the excitation of a fluid-loaded plate by a random pressure field is presented, and formulations for the power quantities of interest are obtained. Additionally, an exact characterization of the nature of the acoustic coupling is presented, demonstrating that it is too simplistic to consider it solely as a mechanism for transferring energy between modes. In §3 the asymptotic evaluation of the coupling terms is described. The analysis itself is lengthy, and the section is written so that this part may be omitted without affecting the arguments put forward in §4, where the full and approximate solutions for the relevant power quantities are compared. The comparison extends from overall powers down to individual modal powers, and includes detailed explanations of the individual modal behaviour via a model that considers interactions between two modes only. This allows the identification of the important differences when coupling is neglected, and hence the requirements for these to be negligible. The section concludes with the new SEA expressions for the significantly fluid-loaded plate, and comparisons of SEA and modal predictions.

Finally the conclusions of the work, and how they apply to a broader class of problems, are discussed in §5. Although the results in §4 are obtained for a specific, and somewhat limited, situation, it is argued that they have a wider applicability and may thus be used as general requirements for the neglect of coupling by an ambient fluid.

2. The boundary-layer excited plate

(*a*) *Introduction*

The model problem is shown in figure 1. Here a simply supported thin elastic plate, of length a, breadth b, mass per unit area M and bending stiffness B ($= Eh^3/12(1-\nu^2)$ in terms of the Young modulus E, thickness h and Poisson ratio ν), is excited by a turbulent boundary layer and radiates acoustic power into the bounding fluid (density ρ_0, sound speed c_0). Surrounding the plate is an infinite rigid baffle, and backing it is a vacuum.

The problem is solved under the assumption that the interaction between boundary-layer and acoustic pressures is negligible, so that the surface pressure

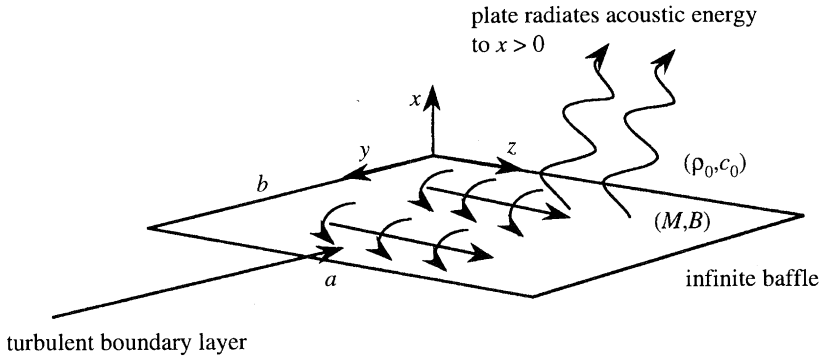

Figure 1. The boundary-layer excited plate. Set in an infinite rigid baffle, with simply supported edges, the plate is driven by the turbulence pressures on its surface and radiates acoustic energy into the surrounding fluid.

fluctuation on the plate consists of the sum of the 'blocked' (rigid wall) turbulent boundary-layer pressure and the acoustic pressure due to the plate motion. The coupled fluid–plate response may then be found by expanding the plate displacement in terms of its modes of vibration *in vacuo* and solving for the modal velocities. The analysis is well known (see, for example, Davies 1971*a*; Lomas & Hayek 1977) and will only be summarized here, to introduce notation and provide a basis for the discussion of power quantities in §2*c*.

(*b*) *Analysis*

As our aim is to derive power spectra, the analysis is in terms of variables Fourier-transformed with respect to time. The plate displacement component $w(y, z, \omega)\, \mathrm{e}^{-\mathrm{i}\omega t}\, \mathrm{d}\omega/2\pi$ is then determined by the single-frequency response equation

$$(B\nabla^4 - M\omega^2)\, w = -p_t - p_0, \tag{2.1}$$

where $p_t(x, y, z, \omega)$ and $p_0(x, y, z, \omega)$ are the boundary-layer and acoustic pressures. For a flow of low Mach number, p_0 satisfies the Helmholtz equation

$$(\nabla^2 + k_0^2)\, p_0 = 0 \tag{2.2}$$

(here $k_0 = \omega/c_0$, the acoustic wavenumber), and the problem specification is completed by the boundary condition linking fluid and plate displacements,

$$\partial p_0/\partial x|_{x=0} = \rho_0\, \omega^2 w. \tag{2.3}$$

On performing the modal analysis, the response equation, (2.1), is found to take the matrix form

$$d_{mn}\, v_{mn} + \epsilon_{f0} \sum_{p,q}{}' Z^{0f}_{mnpq}\, v_{pq} = -p_{tmn}/M\omega. \tag{2.4}$$

Here p_{tmn} and v_{mn} are the components of the turbulence pressure and plate velocity in the (m, n) mode, e.g.

$$p_{tmn}(\omega) = \int_0^a \int_0^b p_t(0, y, z, \omega)\, \Psi_{mn}(y, z)\, \mathrm{d}y\, \mathrm{d}z, \tag{2.5}$$

with

$$\Psi_{mn}(y, z) = [2/\sqrt{(ab)}] \sin k_m z \sin k_n y \tag{2.6}$$

in terms of the modal wavenumbers $k_m = m\pi/a, k_n = n\pi/b$. The acoustic pressure

contributes via the fluid-loading parameter $\epsilon_{f0} = \rho_0 c_0/M\omega$, and the dimensionless impedances Z^{0f}_{mnpq}, which describe the contribution of the (p, q) modal velocity to the (m, n) modal pressure as follows:

$$p_{0mn} = \rho_0 c_0 \sum_{p,q} Z^{0f}_{mnpq} v_{pq}. \tag{2.7}$$

Equation (2.7) is derived from (2.2) and (2.3) by taking Fourier transforms in the spatial variables y and z, so that Z^{0f}_{mnpq} takes the integral form

$$Z^{0f}_{mnpq} = \frac{k_0}{(2\pi)^2} \int_{-\infty}^{\infty} \int_{-\infty}^{\infty} \frac{S^*_{mn}(k_y, k_z) S_{pq}(k_y, k_z)}{(k_0^2 - k_y^2 - k_z^2)^{\frac{1}{2}}} \, \mathrm{d}k_y \, \mathrm{d}k_z, \tag{2.8}$$

where (for positive ω) the square root must be either positive real or positive imaginary, to satisfy the requirements of causality and boundedness for the acoustic field, and the shape functions S_{mn}, S_{pq} are the spatial Fourier transforms of the corresponding mode shapes:

$$S_{mn}(k_y, k_z) = \int_0^a \int_0^b \Psi_{mn}(y, z) \, \mathrm{e}^{-\mathrm{i}k_y y} \, \mathrm{e}^{-\mathrm{i}k_z z} \, \mathrm{d}y \, \mathrm{d}z. \tag{2.9}$$

This integral may be evaluated analytically and we find that, for $(m+p)$ odd, the product $S^*_{mn} S_{pq}$ is an odd function of k_z, and is similarly odd in k_y for $(n+q)$ odd. The modal acoustic impedance Z^{0f}_{mnpq} is thus zero unless $(m+p)$ and $(n+q)$ are both even, in which case the product is purely real, and the real and imaginary parts of Z^{0f}_{mnpq} arise from the supersonic $(k_y^2 + k_z^2 < k_0^2)$ and subsonic $(k_y^2 + k_z^2 > k_0^2)$ integration ranges respectively.

The prime on the summation in (2.4) signifies that the term $Z^{0f}_{mnmn} v_{mn}$ is excluded, Z^{0f}_{mnmn} instead being combined with the structural parameters in the dimensionless impedance

$$d_{mn} = \mathrm{i}[(k^4_{mn}/n^4_{\mathrm{p}})(1 - \mathrm{i}\epsilon_{\mathrm{s}}) - 1] + \epsilon_{f0} Z^{0f}_{mnmn}. \tag{2.10}$$

Here $k_{mn} = (k_m^2 + k_n^2)^{\frac{1}{2}}$ is the overall modal wavenumber, $n_{\mathrm{p}} = (M\omega^2/B_{\mathrm{r}})^{\frac{1}{4}}$ the plate wavenumber, and structural damping has been represented by the addition of a small imaginary part to the plate bending stiffness, $B = B_{\mathrm{r}}(1 - \mathrm{i}\epsilon_{\mathrm{s}})$.

An exact solution to (2.4) may only be found numerically. A common approximation is to neglect the coupling terms, and thereby obtain the explicit result $M\omega v_{mn} = -p_{\mathrm{t}mn}/d_{mn}$. In this work, however, we retain the full equations and derive the relevant power spectra in terms of the (as yet unknown) coupled solution

$$M\omega v_{mn} = \sum_{p,q} Y_{mnpq}(-p_{\mathrm{t}pq}). \tag{2.11}$$

(c) *Power calculations*

(i) *Power spectra*

The spectrum of the radiated acoustic power, $S_0(\omega)$, is given by

$$2\pi \, \delta(\omega - \omega') S_0(\omega) = \int_0^a \int_0^b 2\mathrm{Re}\,[\overline{p_0(0, y, z, \omega) \, v^*(y, z, \omega')}] \, \mathrm{d}y \, \mathrm{d}z, \tag{2.12}$$

where the overbar denotes an ensemble average and $\delta(\,)$ is the Dirac delta function.

On expressing the pressure and velocity as modal sums, performing the integration and using (2.7), (2.11), we find

$$S_0(\omega) = \sum_{m,n} S_{0mn}(\omega), \tag{2.13}$$

where S_{0mn} is the spectrum of the radiation from mode (m, n), given by

$$M\omega S_{0mn}(\omega) = 2\epsilon_{f0} \sum_{p,q} \sum_{r,s} \sum_{i,j} \mathrm{Re}\,[Z^{0f}_{mnpq}\, Y_{pqrs}\, Y^*_{mnij}\, \Phi_{rsij}]. \tag{2.14}$$

Here Φ_{rsij} is the cross-modal excitation, defined in terms of the wavenumber-frequency spectrum of the turbulence pressures, $\Phi_p(k_y, k_z, \omega)$:

$$\Phi_{rsij}(\omega) = \frac{1}{(2\pi)^2} \int_{-\infty}^{\infty} \int_{-\infty}^{\infty} \Phi_p(k_y, k_z, \omega)\, S^*_{rs}(k_y, k_z)\, S_{ij}(k_y, k_z)\, \mathrm{d}k_y\, \mathrm{d}k_z. \tag{2.15}$$

The corresponding spectra for the boundary-layer input and structurally dissipated powers, S_{tmn} and S_{dmn}, are best obtained by multiplying (2.4) by $v^*_{mn}(\omega')$, ensemble averaging and again applying (2.11). The result is the modal power balance equation, $S_{tmn} = S_{0mn} + S_{dmn}$, where

$$M\omega S_{tmn}(\omega) = 2 \sum_{p,q} \mathrm{Re}\,[Y^*_{mnpq}\, \Phi_{mnpq}] \tag{2.16}$$

and

$$M\omega S_{dmn}(\omega) = 2\epsilon_s \frac{k^4_{mn}}{n^4_p} \sum_{p,q} \sum_{r,s} Y_{mnpq}\, Y^*_{mnrs}\, \Phi_{pqrs}. \tag{2.17}$$

The overall power balance equation, $S_t = S_0 + S_d$, is trivially confirmed by summation.

(ii) *The diagonal approximation*

For comparison purposes we require expressions for S_{tmn}, S_{0mn} and S_{dmn} when coupling terms are neglected. Then $Z^{0f}_{mnpq} = Z^{0f}_{mnmn}\, \delta_{mp}\, \delta_{nq}$, and (2.11) takes the form $Y_{mnpq} = d^{-1}_{mn} \delta_{mp}\, \delta_{nq}$. (Here δ_{ij} is the Kronecker delta, equal to one for $i = j$, and zero otherwise.) Under this approximation, (2.14), (2.16) and (2.17) become

$$M\omega S^d_{tmn}(\omega) = 2(\mathrm{Re}\,[d_{mn}]/|d_{mn}|^2)\, \Phi_{mnmn}, \tag{2.18}$$

$$M\omega S^d_{0mn}(\omega) = 2\epsilon_{f0} \frac{\mathrm{Re}\,[Z^{0f}_{mnmn}]}{|d_{mn}|^2} \Phi_{mnmn}, \tag{2.19}$$

$$M\omega S^d_{dmn}(\omega) = 2\epsilon_s \frac{k^4_{mn}}{n^4_p} \frac{\Phi_{mnmn}}{|d_{mn}|^2}, \tag{2.20}$$

and the modal power balance is clearly preserved here.

Some authors, for example Davies (1971*a*), Keltie & Peng (1987), present an analysis that allows coupling to be important in the power quantities even if it has been neglected in solving for the plate response. This approach applies if the coupling impedances are comparable with Z^{0f}_{mnmn}, but fluid-loading is so light that the structural properties dominate (2.4). The diagonal approximation above is then only valid if there is no significant coupling in the excitation terms: $\Phi_{mnpq} = \Phi_{mnmn}\, \delta_{mp}\, \delta_{nq}$.

(iii) *The nature of the acoustic coupling*

In cases where the coupling is important, it is instructive to consider its characteristics. To do so, we write (2.14) for the (m, n) radiated power spectrum as a sum of interactions S^{pq}_{0mn} with modes (p, q). These terms are given by

$$M\omega S^{pq}_{0mn}(\omega) = 2\epsilon_{f0}\,\mathrm{Re}\,[Z^{0f}_{mnpq}\,V_{pqmn}], \tag{2.21}$$

where

$$V_{pqmn} = \sum_{r,s}\sum_{i,j} Y_{pqrs}\,Y^{*}_{mnij}\,\Phi_{rsij} \tag{2.22}$$

is a quantity proportional to the cross-spectrum of the (m, n) and (p, q) velocities. The reverse interaction, S^{mn}_{0pq}, may be related to S^{pq}_{0mn} by using symmetry properties of the problem. First, because the shape function product in the integrals for Z^{0f}_{mnpq} and Φ_{rsij} ((2.8) and (2.15)) is real, $Z^{0f}_{pqmn} = Z^{0f}_{mnpq}$ and $\Phi_{ijrs} = \Phi_{rsij}$. Furthermore, as the wavenumber-frequency spectrum of the turbulence pressures, $\Phi_p(k_y, k_z, \omega)$, is also real, $\Phi^{*}_{rsij} = \Phi_{rsij}$. Thus we find

$$M\omega S^{pq}_{0mn}(\omega) = 2\epsilon_{f0}[\mathrm{Re}\,(Z^{0f}_{mnpq})\,\mathrm{Re}\,(V_{pqmn}) - \mathrm{Im}\,(Z^{0f}_{mnpq})\,\mathrm{Im}\,(V_{pqmn})], \tag{2.23a}$$

$$M\omega S^{mn}_{0pq}(\omega) = 2\epsilon_{f0}[\mathrm{Re}\,(Z^{0f}_{mnpq})\,\mathrm{Re}\,(V_{pqmn}) + \mathrm{Im}\,(Z^{0f}_{mnpq})\,\mathrm{Im}\,(V_{pqmn})]. \tag{2.23b}$$

Equations (2.23) represent a coupling with two parts: 'leaky' and 'direct'. The imaginary part of Z^{0f}_{mnpq} leads to the direct coupling, which is of opposite sign in (2.23*a*) and (2.23*b*) and represents energy transfer between the modes. This is an effect one would naturally associate with coupling. The real part of Z^{0f}_{mnpq}, on the other hand, leads to a term that is of the same sign for each mode, representing energy radiated due to their mutual interaction: leaky coupling. This phenomenon may be explained by noting that the real part of Z^{0f}_{mnpq} arises from the integration range in (2.8) corresponding to supersonic (i.e. radiating) wavenumbers, and is thus associated with a field carrying energy away from the plate. By contrast, the imaginary part arises from subsonic, non-radiating wavenumbers, whose field can only transfer energy from one mode to another: direct coupling.

The general analysis presented here already shows that the modal coupling provided by the acoustic field is somewhat unusual. Later, in §4, we shall find that it is also on occasion highly counter-intuitive, because the leaky coupling terms can become negative, corresponding to both modes extracting energy from the ambient acoustic field. To proceed further at this point it is necessary to evaluate the impedance Z^{0f}_{mnpq}, and this is the subject of the following section.

3. Evaluation of the modal acoustic impedance

(*a*) *Introduction*

Numerical evaluation of Z^{0f}_{mnpq} is computationally arduous for cases with $m \neq p$, $n \neq q$, particularly at high mode numbers. The successful solution of the coupled response equations (2.4) in situations involving many modes thus rests on finding accurate analytical approximations to the impedance.

Some such approximations already exist. The real part of the direct impedance, Z^{0f}_{mnmn}, has been comprehensively characterized by Leppington *et al.* (1982), and its imaginary part is known to leading order for modes shorter than the acoustic wavelength (Davies 1971*a*; Chang & Leehey 1979). However, in spite of the efforts

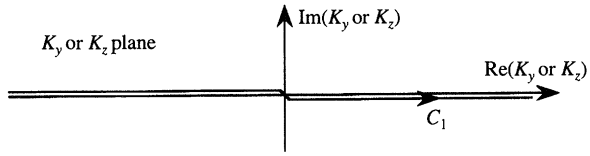

Figure 2. Integration contour C_1. The K_y and K_z integrals in (3.1) must be deformed onto C_1 to avoid real axis poles, which occur when the oscillatory terms in the integrand are decomposed into their exponential components.

of Davies (1971*b*) and Pope & Leibowitz (1974), no accurate, numerically validated expressions have been found for the coupling cases ($m \neq p$ and/or $n \neq q$). The asymptotic analysis presented here remedies this deficiency via a unified approach that not only reproduces and extends the known results for the direct impedance, but also yields new expressions for the coupling impedances. The theory follows Leppington *et al.* (1982, 1986) in considering the high-frequency case, where the products $k_0 a$, $k_0 b$ of the acoustic wavenumber and the plate dimensions are large, and is presented in §§3*b*–3*d*. The results are summarized and compared with numerical evaluations of the integral in §3*e*.

(*b*) *Preliminary analysis*

The natural length scale for the impedance integral is k_0^{-1}, and all wavenumbers will be non-dimensionalized accordingly. Thus, writing $k_y = k_0 K_y$, $k_z = k_0 K_z$, (2.8) becomes

$$Z^{0f}_{mnpq} = \frac{1}{(2\pi)^2} \int_{-\infty}^{\infty} \int_{-\infty}^{\infty} \frac{k_0^2 S^*_{mn}(k_0 K_y, k_0 K_z)\, S_{pq}(k_0 K_y, k_0 K_z)}{(1-K_y^2-K_z^2)^{\frac{1}{2}}} \,\mathrm{d}K_y \,\mathrm{d}K_z. \tag{3.1}$$

The evaluation of the shape function product for $(m+p)$, $(n+q)$ even is straightforward, yielding an oscillatory expression dependent on K_y, K_z, the dimensionless modal wavenumbers K_m, K_n, K_p, K_q, and the dimensionless plate length, $\mu = k_0 a$, and breadth, $\eta = k_0 b$ (Graham 1993). On decomposing the oscillating terms into their exponential components, (3.1) may be cast in a form suitable for contour integration, namely

$$Z^{0f}_{mnpq} = \frac{4K_m K_n K_p K_q}{\pi^2 \mu \eta} \int_{C_1} \int_{C_1} \frac{F_{1mp}(K_z)\, G_{1nq}(K_y)}{(1-K_y^2-K_z^2)^{\frac{1}{2}}} \,\mathrm{d}K_y \,\mathrm{d}K_z, \tag{3.2}$$

where
$$F_{1mp}(K_z) = [1-(-1)^m \,\mathrm{e}^{\mathrm{i}\mu K_z}]/[(K_z^2-K_m^2)(K_z^2-K_p^2)] \tag{3.3}$$

and $G_{1nq}(K_y)$ is similarly defined (with μ replaced by η). The integration paths have been deformed onto the contour C_1 (figure 2) to avoid the real-axis singularities introduced by the decomposition when $m = p$ and/or $n = q$.

For $m \neq p$ and $n \neq q$, there is a four-dimensional parameter space for (3.2). Fortunately, this may be reduced by the method used by Leppington *et al.* (1986). When $m \neq p$, but $n = q$, F_{1mp} is written in partial fraction form, yielding

$$Z^{0f}_{mnpn} = [K_m K_p/(K_p^2-K_m^2)][J^{\mathrm{x}}_{pn} - J^{\mathrm{x}}_{mn}], \tag{3.4}$$

where
$$J^{\mathrm{x}}_{mn} = \frac{4K_n^2}{\pi^2 \mu \eta} \int_{C_1} \int_{C_1} \frac{F_m(K_z)\, G_{1nn}(K_y)}{(1-K_y^2-K_z^2)^{\frac{1}{2}}} \,\mathrm{d}K_y \,\mathrm{d}K_z \tag{3.5}$$

and
$$F_m(K_z) = [1-(-1)^m \,\mathrm{e}^{\mathrm{i}\mu K_z}]/(K_z^2-K_m^2). \tag{3.6}$$

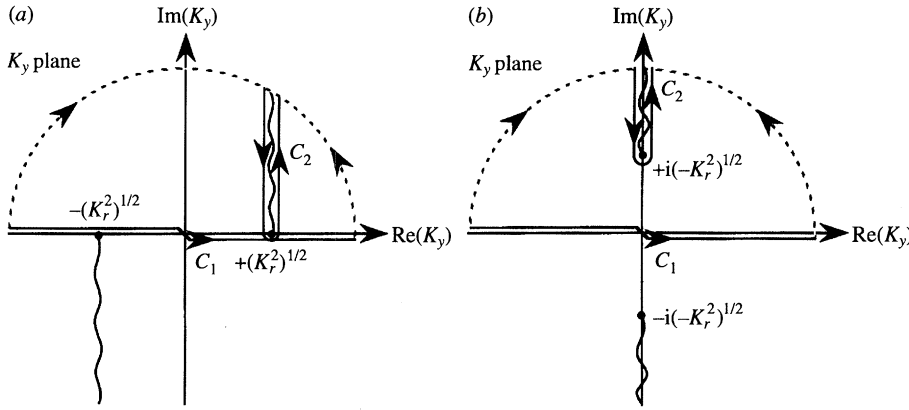

Figure 3. Branch cuts and integration contours in the K_y plane: (*a*) $K_r^2 > 0$; (*b*) $K_r^2 < 0$. For $K_r^2 (= 1 - K_z^2)$ positive, the branch points for $(1 - K_y^2 - K_z^2)^{\frac{1}{2}}$ are at $\pm (K_r^2)^{\frac{1}{2}}$, and for K_r^2 negative they are at $\pm \mathrm{i}(-K_r^2)^{\frac{1}{2}}$. In each case the integration path is deformed onto C_2, the contour around the upper half-plane branch cut.

Similarly, for $m \neq p$ and $n \neq q$,

$$Z^{\mathrm{of}}_{mnpq} = \{K_m K_n K_p K_q / [(K_p^2 - K_m^2)(K_q^2 - K_n^2)]\} [J^{\mathrm{xx}}_{pq} - J^{\mathrm{xx}}_{mq} - J^{\mathrm{xx}}_{pn} + J^{\mathrm{xx}}_{mn}], \tag{3.7}$$

where

$$J^{\mathrm{xx}}_{mn} = \frac{4}{\pi^2 \mu \eta} \int_{C_1} \int_{C_1} \frac{F_m(K_z)\, G_n(K_y)}{(1 - K_y^2 - K_z^2)^{\frac{1}{2}}} \mathrm{d}K_y \, \mathrm{d}K_z \tag{3.8}$$

and $G_n(K_y)$ is defined similarly to $F_m(K_z)$. The remaining case, where $m = p$ and $n \neq q$, may simply be obtained from the $m \neq p$, $n = q$ case by making the appropriate exchanges of variables, so this completes the preliminary analysis required. In the following sections, we perform an asymptotic evaluation of the integrals presented here, under the assumption $\mu, \eta \gg 1$: the high-frequency approximation.

(*c*) *Evaluation of the first integral*

The first integral to be evaluated will usually be that over K_y. The K_y plane branch cuts required to ensure the correct behaviour of the square root term will then depend on K_z via the quantity $K_r^2 = 1 - K_z^2$, taking the form of figure 3(*a*) for $K_r^2 > 0$, and that of figure 3(*b*) for $K_r^2 < 0$. There are two cases to consider; $n = q$ and $n \neq q$.

(i) *The $n = q$ case*

When $n = q$, the integral over K_y is

$$I_{nn}(K_z) = \int_{C_1} \frac{G_{1nn}(K_y)}{(K_r^2 - K_y^2)^{\frac{1}{2}}} \mathrm{d}K_y. \tag{3.9}$$

The integration contour is deformed onto the upper half-plane branch cut, yielding $I_{nn} = I_{nn1} - I_{nn2}$, where

$$I_{nn1} = \frac{\pi \eta}{2K_n^2} \frac{1}{(K_r^2 - K_n^2)^{\frac{1}{2}}} + \int_{C_2} \frac{1}{(K_y^2 - K_n^2)^2} \frac{\mathrm{d}K_y}{(K_r^2 - K_y^2)^{\frac{1}{2}}} \tag{3.10}$$

and

$$I_{nn2} = \int_{C_2} \frac{\mathrm{e}^{\mathrm{i}\eta(K_y - K_n)}}{(K_y^2 - K_n^2)^2} \frac{\mathrm{d}K_y}{(K_r^2 - K_y^2)^{\frac{1}{2}}}. \tag{3.11}$$

The first component, I_{nn1}, may be evaluated exactly, with the following result:

$$I_{nn1} = \frac{\pi\eta}{2K_n^2}\left[\frac{-\mathrm{i}}{(K_n^2-K_r^2)^{\frac{1}{2}}} - \frac{2\mathrm{i}}{\pi\eta(K_n^2-K_r^2)}\left(\frac{2K_n^2-K_r^2}{K_n(K_n^2-K_r^2)^{\frac{1}{2}}}\left\{\ln\left(\frac{K_n+(K_n^2-K_r^2)^{\frac{1}{2}}}{K_r}\right)+\tfrac{1}{2}\mathrm{i}\pi\right\}-1\right)\right], \tag{3.12}$$

where K_r is either positive real or positive imaginary, and $(K_n^2-K_r^2)^{\frac{1}{2}} = -\mathrm{i}(K_r^2-K_n^2)^{\frac{1}{2}}$ for $K_r > K_n$. The second, however, may only be found asymptotically, by expanding the non-exponential terms in the integrand about $K_y = K_r$ and integrating term by term. This process gives

$$I_{nn2} \sim (2\pi/\eta K_r)^{\frac{1}{2}}\mathrm{e}^{-\mathrm{i}\pi/4}\,\mathrm{e}^{i\eta(K_r-K_n)}/(K_r^2-K_n^2)^2 + O(\eta^{-\frac{3}{2}}\mathrm{e}^{\mathrm{i}\eta(K_r-K_n)}) \tag{3.13}$$

unless $K_r \approx K_n$ or $K_r \approx 0$. The latter case will not be required, but the former will, and must be considered more carefully. To account for the rapid variation of (K_y-K_n) at the base of the branch cut, we make the substitutions $K_y = K_r+\mathrm{i}u/\eta$, $K_n = K_r+y/\eta$, and note that the contribution to the integral away from the base is exponentially small. The asymptotic analysis (Graham 1993) then yields

$$I_{nn2} \sim a_1\eta^{\frac{3}{2}} + a_2\eta^{\frac{1}{2}} + O(\eta^{-\frac{1}{2}}), \tag{3.14}$$

where

$$a_1 = -\frac{2^{\frac{1}{2}}\pi^{\frac{1}{2}}\mathrm{e}^{-\mathrm{i}\pi/4}}{K_r^{\frac{1}{2}}(K_r+K_n)^2}\left[\left(2+\frac{i}{y}\right)\left\{\frac{F^*(y^{\frac{1}{2}})}{y^{\frac{1}{2}}} - \frac{\pi^{\frac{1}{2}}\mathrm{e}^{-\mathrm{i}\pi/4}}{2y^{\frac{1}{2}}}\right\} - \frac{\mathrm{i}\mathrm{e}^{-\mathrm{i}y}}{y}\right], \tag{3.15a}$$

$$a_2 = -\frac{\pi^{\frac{1}{2}}\mathrm{e}^{\mathrm{i}\pi/4}(9K_r+K_n)}{2^{\frac{3}{2}}K_r^{\frac{3}{2}}(K_r+K_n)^3}\left[(2\mathrm{i}y+1)\left\{\frac{F^*(y^{\frac{1}{2}})}{y^{\frac{1}{2}}} - \frac{\pi^{\frac{1}{2}}\mathrm{e}^{-\mathrm{i}\pi/4}}{2y^{\frac{1}{2}}}\right\} + \mathrm{e}^{-\mathrm{i}y}\right], \tag{3.15b}$$

$$F^*(z) = \int_0^z \mathrm{e}^{-\mathrm{i}t^2}\,\mathrm{d}t, \tag{3.16}$$

and $y^{\frac{1}{2}}$ is either positive real or negative imaginary.

To complete the analysis for I_{nn2} in the $K_r \approx K_n$ transition region, (3.14) must now be shown to match with the non-uniform approximation, (3.13). Using the Fresnel integral relations in §7.3 of Abramowitz & Stegun (1965), we obtain

$$\frac{F^*(y^{\frac{1}{2}})}{y^{\frac{1}{2}}} - \frac{\pi^{\frac{1}{2}}\mathrm{e}^{-\mathrm{i}\pi/4}}{2y^{\frac{1}{2}}} \sim \frac{\mathrm{i}\mathrm{e}^{-\mathrm{i}y}}{2y} - \frac{\mathrm{e}^{-\mathrm{i}y}}{4y^2} - \frac{3\mathrm{i}\mathrm{e}^{-\mathrm{i}y}}{8y^3} + O(y^{-4}) \tag{3.17}$$

for $|y|$ large. Equations (3.15) thus become

$$a_1 \sim \frac{2^{\frac{1}{2}}\pi^{\frac{1}{2}}\mathrm{e}^{-\mathrm{i}\pi/4}}{K_r^{\frac{1}{2}}(K_r+K_n)^2}\frac{\mathrm{e}^{-\mathrm{i}y}}{y^2} + O(y^{-3}), \quad a_2 \sim O(y^{-2}), \tag{3.18}$$

and, noting that $y = \eta(K_n-K_r)$, it is clear that the expressions for I_{nn2} match in the regions $|y| \gg 1$.

It remains to consider the combined expression, $I_{nn} = I_{nn1}-I_{nn2}$, and demonstrate that the singularities in I_{nn1} at $K_n = K_r$ are cancelled by I_{nn2}. On expressing I_{nn1} in terms of y, we find

$$I_{nn} \sim b_1\eta^{\frac{3}{2}} + b_2\eta^{\frac{1}{2}} + O(\eta^0), \tag{3.19}$$

with

$$b_1 = \frac{2^{\frac{1}{2}}\pi^{\frac{1}{2}}\mathrm{e}^{-\mathrm{i}\pi/4}}{K_r^{\frac{1}{2}}(K_r+K_n)^2}\left[\left(2+\frac{i}{y}\right)\frac{F^*(y^{\frac{1}{2}})}{y^{\frac{1}{2}}} - \frac{\mathrm{i}\mathrm{e}^{-\mathrm{i}y}}{y}\right], \tag{3.20a}$$

PHILOSOPHICAL TRANSACTIONS OF THE ROYAL SOCIETY A MATHEMATICAL, PHYSICAL & ENGINEERING SCIENCES

and
$$b_2 = \frac{\pi^{\frac{1}{2}} e^{i\pi/4}(9K_r + K_n)}{2^{\frac{3}{2}} K_r^{\frac{3}{2}}(K_r + K_n)^3}\left[(2iy+1)\frac{F^*(y^{\frac{1}{2}})}{y^{\frac{1}{2}}} + e^{-iy}\right] \tag{3.20b}$$

around $K_r = K_n$. The small argument form of the Fresnel integral,

$$F^*(z) = z - \tfrac{1}{3}iz^3 + O(z^5), \tag{3.21}$$

may then be used to show that (3.19) is analytic at $y = 0$.

(ii) *The $n \neq q$ case*

The integral over K_y is now

$$I_n = \int_{C_1} \frac{G_n(K_y)}{(K_r^2 - K_y^2)^{\frac{1}{2}}} \mathrm{d}K_y, \tag{3.22}$$

and the same approach as for I_{nn} yields $I_n = I_{n1} - I_{n2}$, where I_{n1} takes the exact form

$$I_{n1} = \frac{2i}{K_n(K_n^2 - K_r^2)^{\frac{1}{2}}}\left[\ln\left(\frac{K_n + (K_n^2 - K_r^2)^{\frac{1}{2}}}{K_r}\right) + \tfrac{1}{2}i\pi\right] \tag{3.23}$$

and
$$I_{n2} \sim \left(\frac{2\pi}{\eta K_r}\right)^{\frac{1}{2}} \frac{e^{-i\pi/4}\, e^{i\eta(K_r - K_n)}}{K_r^2 - K_n^2} + O(\eta^{-\frac{3}{2}} e^{i\eta(K_r - K_n)}) \tag{3.24}$$

away from the regions $K_r \approx 0$ and $K_r \approx K_n$. In the latter,

$$I_{n2} \sim \frac{2^{\frac{3}{2}}\pi^{\frac{1}{2}} e^{i\pi/4}\eta^{\frac{1}{2}}}{K_r^{\frac{1}{2}}(K_r + K_n)}\left[\frac{F^*(y^{\frac{1}{2}})}{y^{\frac{1}{2}}} - \frac{\pi^{\frac{1}{2}} e^{-i\pi/4}}{2y^{\frac{1}{2}}}\right] + O(\eta^{-\frac{1}{2}}), \tag{3.25}$$

which may be demonstrated to match with (3.24) by using the same method as previously. Additionally, the singularity at $y = 0$ in (3.25) cancels that in I_{n1}, and I_n is thus analytic at $K_r = K_n$.

The results for I_{nn} and I_n presented here may be justified by noting that they include, as a special case ($K_r = 1$), the expressions of Leppington *et al.* (1986) for the one-dimensional plate. We thus move on to consider the three cases required for the second integral: direct ($m = p, n = q$), singly-cross ($m \neq p, n = q$) and doubly-cross ($m \neq p, n \neq q$).

(*d*) *Evaluation of the second integral*

In evaluating the K_z integral, it is first necessary to define the K_z plane branch cuts. There are two roots to consider, namely $K_r\,(= (1 - K_z^2)^{\frac{1}{2}})$ and $(K_r^2 - K_n^2)^{\frac{1}{2}}$, both of which are either positive real or positive imaginary for real K_z. The branch cuts in the K_z plane are thus as shown in figures 4 (for $K_n < 1$) and 5 ($K_n > 1$). In addition, we shall need two steepest descent contours, $SD1$ and $SD2$, corresponding to the exponentials $e^{i\eta K_r}$ and $e^{i\mu K_z} e^{i\eta K_r}$. The contours have been calculated by Graham (1993), and are also plotted in figures 4 and 5. (The angle θ_c is defined by $\tan\theta_c = b/a$.)

(i) *Contour deformations*

In all three cases under consideration, the same integrand arrangements and contour deformations will be necessary, so that it will suffice to consider the direct case as a demonstration of the approach employed. Substituting (3.9) into (3.2) gives

$$Z_{mnmn}^{\mathrm{bf}} = \frac{4K_m^2 K_n^2}{\pi^2 \mu\eta} \int_{C_1} F_{1mm}(K_z)\, I_{nn}(K_z)\, \mathrm{d}K_z \tag{3.26}$$

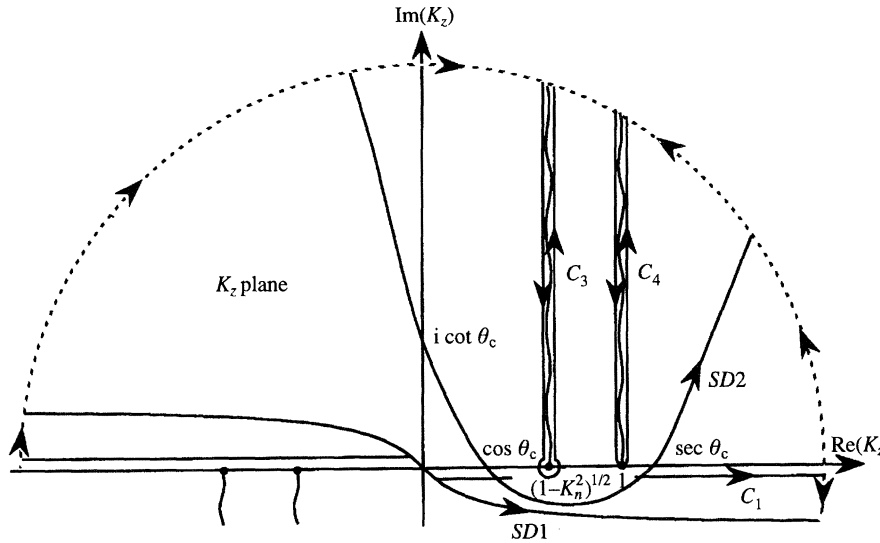

Figure 4. Branch cuts and integration contours in the K_z plane when $K_n < \sin\theta_c$. The integral along C_1 is decomposed into three parts, each of which has its integration path deformed onto a suitable contour. Note that the branch cuts and $SD2$ do not intersect.

for the direct impedance. The integrand must now be split into separate components, each component being deformed onto a suitable contour. The choice of components and subsequent contour deformation is dependent on the location of the $(K_r^2-K_n^2)^{\frac{1}{2}}$ branch cut relative to the contour $SD2$, and there are three distinct ranges of K_n to be considered: $K_n < \sin\theta_c$, $\sin\theta_c < K_n < \operatorname{cosec}\theta_c$ and $K_n > \operatorname{cosec}\theta_c$.

For $K_n < \sin\theta_c$ the branch point at $K_z = (1-K_n^2)^{\frac{1}{2}}$ lies to the right of the saddle point (at $K_z = \cos\theta_c$) on $SD2$. Using $I_{nn} = I_{nn1} - I_{nn2}$ and (3.3) for F_{1mm}, the integral is split into three components:

$$Z^{0f}_{mnmn} = (4K_m^2 K_n^2/\pi^2\mu\eta)[I_{D1} - I_{D2} + I_{D3}], \tag{3.27}$$

where, after the appropriate contour deformations (figure 4), first,

$$I_{D1} = \int_{C_3+C_4} F_{1mm}(K_z)\, I_{nn1}(K_z)\, \mathrm{d}K_z + 2\pi\mathrm{i}R_{D1}, \tag{3.28}$$

with

$$R_{D1} = [(K_z - K_m)\, F_{1mm}(K_z)\, I_{nn1}(K_z)]_{K_z=K_m}; \tag{3.29}$$

secondly,

$$I_{D2} = \int_{SD1} \frac{I_{nn2}(K_z)}{(K_z^2-K_m^2)^2}\, \mathrm{d}K_z; \tag{3.30}$$

and finally,

$$I_{D3} = \int_{SD2} \frac{\mathrm{e}^{\mathrm{i}\mu(K_z-K_m)}}{(K_z^2-K_m^2)^2} I_{nn2}(K_z)\, \mathrm{d}K_z + \delta_m\, 2\pi\mathrm{i}R_{D2}, \tag{3.31}$$

with $\delta_m = H(\cos\theta_c - K_m) + H(K_m - \sec\theta_c)$ and

$$R_{D2} = \left[\frac{\mathrm{d}}{\mathrm{d}K_z}\left\{\frac{\mathrm{e}^{\mathrm{i}\mu(K_z-K_m)}}{(K_z+K_m)^2} I_{nn2}(K_z)\right\}\right]_{K_z=K_m}. \tag{3.32}$$

The residue R_{D2} from the double pole is only picked up if it lies outside the region bounded by the real axis crossings of $SD2$; hence the introduction of the Heaviside step functions in δ_m.

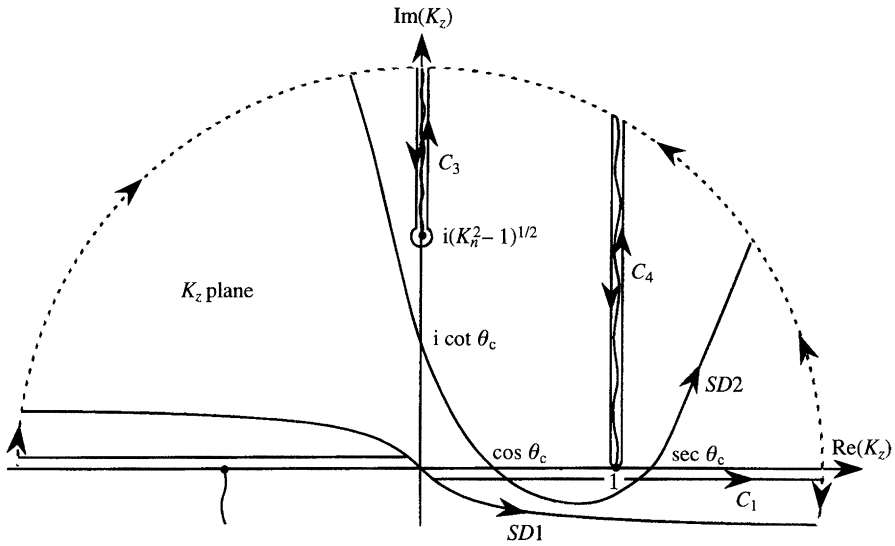

Figure 5. Branch cuts and integration contours in the K_z plane when $K_n > \operatorname{cosec}\theta_c$. As for $K_n < \sin\theta_c$ there is no intersection between $SD2$ and the branch cuts, and the same integral decomposition and contour deformations may be used.

The above formulation also applies for $K_n > \operatorname{cosec}\theta_c$ (figure 5), but when $\sin\theta_c < K_n < \operatorname{cosec}\theta_c$ a different approach to the contour deformation is required, as the steepest descent contour $SD2$ now intersects the first branch cut (figure 6). The integral is written as

$$Z^{0f}_{mnmn} = (4K_m^2 K_n^2/\pi^2\mu\eta)[I_{D4} - I_{D2} - I_{D5}], \tag{3.33}$$

where, after suitable contour deformations, I_{D2} is again defined by (3.30), I_{D4} is given by

$$I_{D4} = \int_{C_3+C_4} \frac{I_{nn1}(K_z)}{(K_z^2-K_m^2)^2}\,\mathrm{d}K_z + 2\pi\mathrm{i}R_{D3}, \tag{3.34}$$

with

$$R_{D3} = \left[\frac{\mathrm{d}}{\mathrm{d}K_z}\left\{\frac{I_{nn1}(K_z)}{(K_z+K_m)^2}\right\}\right]_{K_z=K_m}, \tag{3.35}$$

and I_{D5} by

$$I_{D5} = \int_{SD2+C_{3a}} \frac{\mathrm{e}^{\mathrm{i}\mu(K_z-K_m)}}{(K_z^2-K_m^2)^2} I_{nn}(K_z)\,\mathrm{d}K_z + \delta_m\, 2\pi\mathrm{i}R_{D4}, \tag{3.36}$$

with

$$R_{D4} = \left[\frac{\mathrm{d}}{\mathrm{d}K_z}\left\{\frac{\mathrm{e}^{\mathrm{i}\mu(K_z-K_m)}}{(K_z+K_m)^2} I_{nn}(K_z)\right\}\right]_{K_z=K_m}. \tag{3.37}$$

The contribution to I_{D5} from C_{3a} is exponentially small apart from at the base of the branch cut, where the $K_r \approx K_n$ transition expression, (3.19), applies for I_{nn}. However, noting that $F^*(-z) = -F^*(z)$, it is clear that (3.19) is continuous across the branch cut, at least to the orders of interest, and the integral along C_{3a} can thus be discarded. Now I_{nn} may be split into its component parts, I_{nn1} and I_{nn2}. The integral containing the latter needs no further manipulation, but that involving the

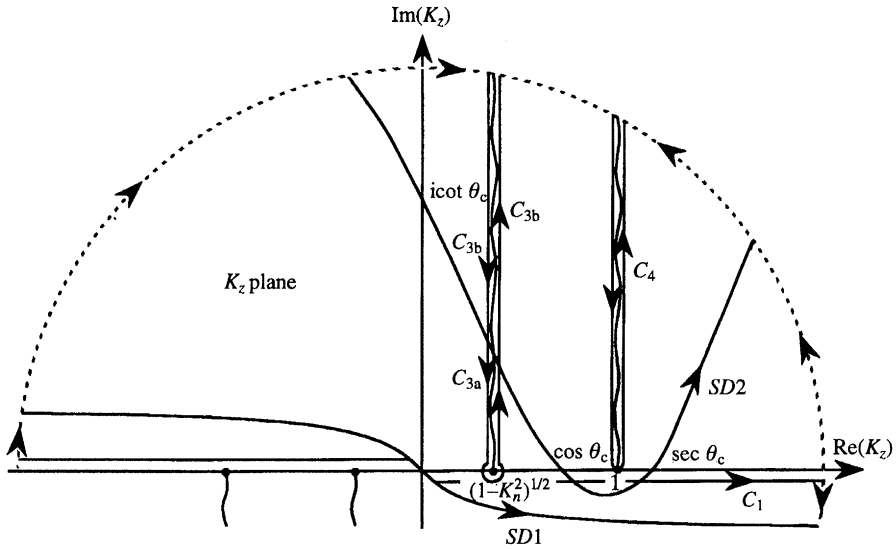

Figure 6. Branch cuts and integration contours in the K_z plane when $\sin\theta_c < K_n < \operatorname{cosec}\theta_c$. The first branch cut and $SD2$ now intersect, necessitating a different approach to the integral decomposition and contour deformations.

former has its integration path further deformed to C_{3b} (the part of the first branch cut above the steepest descent contour) and C_4, giving

$$I_{D5} = \int_{C_{3b}+C_4} \frac{e^{i\mu(K_z-K_m)}}{(K_z^2-K_m^2)^2} I_{nn1}(K_z)\,dK_z - \int_{SD2} \frac{e^{i\mu(K_z-K_m)}}{(K_z^2-K_m^2)^2} I_{nn2}(K_z)\,dK_z + 2\pi i R_{D4} + (1-\delta_m)\,2\pi i R_{D2}. \quad (3.38)$$

It remains to note that R_{D4} may be expressed in terms of R_{D1}, R_{D2} and R_{D3}, namely $R_{D4} = R_{D3} - R_{D1} - R_{D2}$, so that the net residue contributions here will be exactly the same as for the $K_n < \sin\theta_c$, $K_n > \operatorname{cosec}\theta_c$ cases. The results for all three K_n ranges may thus be combined to give

$$Z_{mnmn}^{0f} = Z_{ex} + \delta_m Z_{mo} + \delta_n Z_{no} + Z_{m1} + Z_{n1} + Z_{sd}, \quad (3.39)$$

with δ_n defined similarly to δ_m, being one unless $\sin\theta_c < K_n < \operatorname{cosec}\theta_c$, in which case it is zero, and

$$Z_{ex} = \frac{4K_m^2 K_n^2}{\pi^2\mu\eta}\left\{\int_{C_3+C_4} \frac{I_{nn1}(K_z)}{(K_z^2-K_m^2)^2}\,dK_z + 2\pi i R_{D1}\right\}, \quad (3.40)$$

$$Z_{mo} = (8iK_m^2 K_n^2/\pi\mu\eta)\,R_{D2}, \quad (3.41)$$

$$Z_{no} = -\frac{4K_m^2 K_n^2}{\pi^2\mu\eta}\int_{C_3} \frac{e^{i\mu(K_z-K_m)}}{(K_z^2-K_m^2)^2} I_{nn1}(K_z)\,dK_z, \quad (3.42)$$

$$Z_{m1} = -\frac{4K_m^2 K_n^2}{\pi^2\mu\eta}\int_{C_4} \frac{e^{i\mu(K_z-K_m)}}{(K_z^2-K_m^2)^2} I_{nn1}(K_z)\,dK_z, \quad (3.43)$$

$$Z_{n1} = -(4K_m^2 K_n^2/\pi^2\mu\eta)\,I_{D2} \quad (3.44)$$

and

$$Z_{sd} = \frac{4K_m^2 K_n^2}{\pi^2\mu\eta}\left\{\int_{SD2} \frac{e^{i\mu(K_z-K_m)}}{(K_z^2-K_m^2)^2} I_{nn2}(K_z)dK_z - (1-\delta_n)\int_{C_{3b}} \frac{e^{i\mu(K_z-K_m)}}{(K_z^2-K_m^2)^2} I_{nn1}(K_z)\,dK_z\right\}. \quad (3.45)$$

This general formulation will be used throughout the analysis for the second integral. The problem is thus reduced to the evaluation of the six unknown components of (3.39), and their counterparts for the singly- and doubly-cross cases.

(ii) *Direct case*

Equation (3.40) for $Z_{\rm ex}$ may be evaluated exactly using (3.29) for R_{D1} and (3.12) for I_{nn1}. The integral on C_3 is found to be finite as the radius of the bulb around the I_{nn1} singularity is allowed to tend to zero, and the result is

$$Z_{\rm ex} = -\frac{\mathrm{i}}{P} + \frac{2\mathrm{i}}{\pi P^2}\left\{\frac{A(K_m)}{\mu} + \frac{A(K_n)}{\eta}\right\} + \frac{2}{\pi K_m K_n P^4 \mu\eta} B(K_m, K_n), \tag{3.46}$$

where $P^2 = K_m^2 + K_n^2 - 1$ with P positive real or negative imaginary, $A(K_m)$ is given by

$$A(K_m) = [(K_m^2 + P^2)/K_m Q]\arctan(K_m/Q) + 1, \quad P^2 < 0, Q = \mathrm{i}P, \tag{3.47a}$$

$$A(K_m) = -\frac{(K_m^2 + P^2)}{2K_m P}\left\{\ln\left|\frac{K_m + P}{K_m - P}\right| + \epsilon_{1n}\,\mathrm{i}\pi\right\} + 1, \quad P^2 > 0, \tag{3.47b}$$

with $\epsilon_{1n} = H(1 - K_n)$, $A(K_n)$ and ϵ_{1m} are similarly defined, and finally

$$B(K_m, K_n) = \frac{K_m K_n (2P^4 + P^2 - 3K_m^2 K_n^2)}{(1 - K_m^2)(1 - K_n^2)} - \frac{(2P^4 + P^2 + 3K_m^2 K_n^2)}{Q}\arctan\left(\frac{K_m K_n}{Q}\right), \quad P^2 < 0, Q = \mathrm{i}P, \tag{3.48a}$$

$$B(K_m, K_n) = \frac{K_m K_n (2P^4 + P^2 - 3K_m^2 K_n^2)}{(1 - K_m^2)(1 - K_n^2)} + \frac{(2P^4 + P^2 + 3K_m^2 K_n^2)}{2P}\left\{\ln\left|\frac{K_m K_n + P}{K_m K_n - P}\right| + (\epsilon_{1m} + \epsilon_{1n} - 1)\,\mathrm{i}\pi\right\}, \quad P^2 > 0. \tag{3.48b}$$

The second term in (3.39), Z_{m0}, is defined by (3.41) and is easily evaluated to leading order by using (3.32) and (3.13) for R_{D2} and I_{nn2}, giving, for $K_m < 1$,

$$Z_{m0} \sim -2^{\frac{3}{2}} \mathrm{e}^{-\mathrm{i}\pi/4}\, \mathrm{e}^{\mathrm{i}\eta[L_m - K_n]} K_n^2 (1 - r_2)/\pi^{\frac{1}{2}} L_m^{\frac{1}{2}} P^4 \eta^{\frac{3}{2}} + O(N^{-\frac{5}{2}}) \tag{3.49}$$

where $L_m = (1 - K_m^2)^{\frac{1}{2}}$, $r_2 = \eta K_m/\mu L_m$ and $N = (\mu^2 + \eta^2)^{\frac{1}{2}}$. For $K_m > 1$, Z_{m0} is exponentially small, and we may thus replace $\delta_m Z_{m0}$ in (3.39) with $\epsilon_m Z_{m0}$, where $\epsilon_m = H(\cos\theta_{\rm c} - K_m)$.

Equation (3.49) becomes non-uniform around $P^2 = 0$ (the coincidence transition), and here the $K_r \approx K_n$ form of I_{nn2}, equation (3.14), must be used, leading to

$$Z_{m0} \sim \frac{2^{\frac{3}{2}} \mathrm{e}^{-\mathrm{i}\pi/4} K_n^2 \eta^{\frac{1}{2}}}{\pi^{\frac{1}{2}} L_m^{\frac{1}{2}} (K_n + L_m)^2}\left[\left\{\left(2 + \frac{\mathrm{i}}{z_2}\right)\left(\frac{F^*(z_2^{\frac{1}{2}})}{z_2^{\frac{1}{2}}} - \frac{\pi^{\frac{1}{2}} \mathrm{e}^{-\mathrm{i}\pi/4}}{2z_2^{\frac{1}{2}}}\right) - \frac{\mathrm{i}\mathrm{e}^{-\mathrm{i}z_2}}{z_2}\right\} + r_2\left\{\left(\frac{\mathrm{i}}{z_2} - \frac{3}{2z_2^2}\right)\left(\frac{F^*(z_2^{\frac{1}{2}})}{z_2^{\frac{1}{2}}} - \frac{\pi^{\frac{1}{2}} \mathrm{e}^{-\mathrm{i}\pi/4}}{2z_2^{\frac{1}{2}}}\right) + \frac{3}{2}\frac{\mathrm{e}^{-\mathrm{i}z_2}}{z_2^2}\right\}\right] + O(N^{-\frac{1}{2}}), \tag{3.50}$$

where $z_2 = \eta(K_n - L_m)$. Matching between (3.49) and (3.50) in the regions $|z_2| \gg 1$ may be demonstrated by using (3.17).

The next term, Z_{no}, arises from the branch cut integral given by (3.42). Its asymptotic evaluation is complicated by the singularities in I_{nn1} at the base of the cut, but the result is found to be finite as the radius of the bulb at $K_r = K_n$ tends to zero and, for $K_n < 1$,

$$Z_{no} \sim -2^{\frac{3}{2}} \mathrm{e}^{-\mathrm{i}\pi/4} \mathrm{e}^{\mathrm{i}\mu[L_n - K_m]} K_m^2 (1-r_1)/\pi^{\frac{1}{2}} L_n^{\frac{1}{2}} P^4 \mu^{\frac{3}{2}} + O(N^{-\frac{5}{2}}), \tag{3.51}$$

where $L_n = (1-K_n^2)^{\frac{1}{2}}$ and $r_1 = \mu K_n/\eta L_n$, while for $K_n > 1$, Z_{no} is exponentially small. As with $\delta_m Z_{mo}$, we may thus replace $\delta_n Z_{no}$ with $\epsilon_n Z_{no}$, where $\epsilon_n = H(\sin\theta_c - K_n)$.

Equation (3.51) for Z_{no} is symmetrical with (3.49), in that exchanging μ for η and K_m for K_n will convert Z_{no} to Z_{mo}. The near coincidence form of Z_{no} may thus be obtained either by this straightforward method, or by making the substitutions $K_z = L_n + z/\mu$, $K_m = L_n + z_1/\mu$ and again performing the integral over C_3. In this case,

$$Z_{no} \sim \frac{2^{\frac{3}{2}} \mathrm{e}^{-\mathrm{i}\pi/4} K_m^2 \mu^{\frac{1}{2}}}{\pi^{\frac{1}{2}} L_n^{\frac{1}{2}} (K_m + L_n)^2} \left[\left\{ \left(2 + \frac{i}{z_1}\right) \left(\frac{F^*(z_1^{\frac{1}{2}})}{z_1^{\frac{1}{2}}} - \frac{\pi^{\frac{1}{2}} \mathrm{e}^{-\mathrm{i}\pi/4}}{2 z_1^{\frac{1}{2}}} \right) - \frac{\mathrm{i}\mathrm{e}^{-\mathrm{i}z_1}}{z_1} \right\} \right.$$
$$\left. + r_1 \left\{ \left(\frac{\mathrm{i}}{z_1} - \frac{3}{2z_1^2} \right) \left(\frac{F^*(z_1^{\frac{1}{2}})}{z_1^{\frac{1}{2}}} - \frac{\pi^{\frac{1}{2}} \mathrm{e}^{-\mathrm{i}\pi/4}}{2 z_1^{\frac{1}{2}}} \right) + \frac{3}{2} \frac{\mathrm{e}^{-\mathrm{i}z_1}}{z_1^2} \right\} \right] + O(N^{-\frac{1}{2}}), \tag{3.52}$$

and the comments on matching for Z_{mo} apply in equal measure here.

The Z_{m1} term in (3.39) is the integral around the second branch cut with the same integrand as Z_{no}. It may be evaluated asymptotically, with (negligible) result

$$Z_{m1} \sim 8\mathrm{i}\, \mathrm{e}^{\mathrm{i}\mu(1-K_m)} K_m^2 / \pi K_n^2 (1-K_m^2)^2 \mu^2 \eta \tag{3.53}$$

for K_m not too close to one, nor K_n to zero. If K_m is near one, the integral may be estimated by using the substitutions $K_z = 1 + z/\mu$, $K_m = 1 + x_m/\mu$, which give

$$Z_{m1} \sim -\frac{8K_m^2}{\pi K_n^2 (1+K_m)^2 \eta} \left[\left(\mathrm{i} F_{\mathrm{cs}}(x_m) + \frac{\mathrm{e}^{-\mathrm{i}x_m}}{x_m} \right) \right.$$
$$\left. - \frac{2}{\mu} \left(\frac{1}{K_n^2} + \frac{1}{1+K_m} \right) [(1 + \mathrm{i}x_m) F_{\mathrm{cs}}(x_m) + \mathrm{e}^{-\mathrm{i}x_m}] \right] + O(N^{-3}), \tag{3.54}$$

where

$$F_{\mathrm{cs}}(x) = \mathrm{Ci}(|x|) + \mathrm{i}(\tfrac{1}{2}\pi \operatorname{sgn} x - \mathrm{Si}(x)) \tag{3.55}$$

and Ci, Si are the cosine and sine integrals (see Abramowitz & Stegun (1965), §5.2). For large $|x|$,

$$F_{\mathrm{cs}}(x) \sim \mathrm{i}\, \mathrm{e}^{-\mathrm{i}x}/x - \mathrm{e}^{-\mathrm{i}x}/x^2 + O(x^{-3}) \tag{3.56}$$

and (3.54) thus matches with (3.53) for $|x_m| \gg 1$. Additionally, the discontinuities and singularities in Z_{m1} at $x_m = 0$ exactly cancel those in Z_{ex}, providing a smooth transition through the $K_m = 1$ region.

Alternatively, for K_n close to zero, the substitution $K_n^3 = 2v_n^2/\mu$ replaces $K_m = 1 + x_m/\mu$, and the result is

$$Z_{m1} \sim \frac{4\, \mathrm{e}^{\mathrm{i}\mu(1-K_m)} K_m^2}{\pi (1-K_m^2)^2 \mu \eta} \left[1 - \frac{\mathrm{e}^{-\mathrm{i}\pi/4}(1 + 2\mathrm{i}v_n^2)}{2\pi^{\frac{1}{2}} v_n} I_{F3}(v_n) \right] + O(N^{-3}), \tag{3.57}$$

where

$$I_{F3}(x) = 2\pi^{\frac{1}{2}} \mathrm{e}^{\mathrm{i}\pi/4} \mathrm{e}^{-\mathrm{i}x^2} \operatorname{sgn} x \{ [F^*(|x|)]^* - \tfrac{1}{2}\pi^{\frac{1}{2}} \mathrm{e}^{\mathrm{i}\pi/4} \} \tag{3.58}$$

(the $x < 0$ form will be required in a later expression). For v_n large, matching with

(3.53) may be demonstrated by using (3.17). Analytical expressions have not been found for the case where both $K_m \approx 1$ and $K_n \approx 0$, and we note this as an unresolved problem. The solution is described later, in §3*e*.

The fifth term, Z_{n1}, is the integral along the steepest descent contour $SD1$ and, using (3.13) for I_{nn2}, it may be evaluated via the standard steepest descent technique, with result

$$Z_{n1} \sim 8\mathrm{i}\,\mathrm{e}^{\mathrm{i}\eta(1-K_n)}K_n^2/\pi K_m^2(1-K_n^2)^2\mu\eta^2. \tag{3.59}$$

It is readily apparent that Z_{n1} is the analogue of Z_{m1}, with (3.59) being identical to (3.53) when K_m, K_n and μ, η are exchanged. Like Z_{m1}, Z_{n1} is negligible to the orders of interest unless either K_n is close to one, when

$$Z_{n1} \sim -\frac{8K_n^2}{\pi K_m^2(1+K_n)^2\mu}\left[\left(\mathrm{i}F_{\mathrm{cs}}(x_n)+\frac{\mathrm{e}^{-\mathrm{i}x_n}}{x_n}\right)\right.$$
$$\left.-\frac{2}{\eta}\left(\frac{1}{K_m^2}+\frac{1}{1+K_n}\right)[(1+\mathrm{i}x_n)F_{\mathrm{cs}}(x_n)+\mathrm{e}^{-\mathrm{i}x_n}]\right]+O(N^{-3}), \tag{3.60}$$

with $x_n = \eta(K_n-1)$, or K_m is close to zero, in which case

$$Z_{n1} \sim \frac{4\,\mathrm{e}^{\mathrm{i}\eta(1-K_n)}K_n^2}{\pi(1-K_n^2)^2\mu\eta}\left[1-\frac{\mathrm{e}^{-\mathrm{i}\pi/4}(1+2\mathrm{i}v_m^2)}{2\pi^{\frac{1}{2}}v_m}I_{F3}(v_m)\right]+O(N^{-3}), \tag{3.61}$$

with $v_m = (\eta/2)^{\frac{1}{2}}K_m$. Equations (3.60) and (3.61) are awkward to obtain from the steepest descent integral, whereas their derivation from the symmetry argument is trivial.

Lastly, (3.45) for Z_{sd} consists of a steepest descent integral on contour $SD2$, usually $O(N^{-3})$, and a branch cut integral on $C_{3\mathrm{b}}$ that is exponentially small unless $SD2$ crosses the branch cut very close to the real K_z axis. This term is thus usually negligible, but it becomes important if K_m is close to $\cos\theta_{\mathrm{c}}$, or K_n to $\sin\theta_{\mathrm{c}}$. The two cases may be combined by writing $K_m = \cos\theta_{\mathrm{c}} + 2^{\frac{1}{2}}\sin\theta_{\mathrm{c}}\,y_m/N^{\frac{1}{2}}$, $K_n = \sin\theta_{\mathrm{c}} + 2^{\frac{1}{2}}\cos\theta_{\mathrm{c}}\,y_n/N^{\frac{1}{2}}$ and making the substitution

$$K_z = \cos\theta_{\mathrm{c}} + 2^{\frac{1}{2}}\mathrm{e}^{-\mathrm{i}\pi/4}\sin\theta_{\mathrm{c}}\,v/N^{\frac{1}{2}}.$$

For $|y_n| \sim O(1)$ or larger, the non-uniform expression for I_{nn2}, (3.13), is valid everywhere on $SD2$, and the integral on $C_{3\mathrm{b}}$ is exponentially small. Equation (3.45) then becomes

$$Z_{\mathrm{sd}} \sim [C_{\mathrm{dsd}}/(y_m+y_n)^3N][I_{F3}(y_m)+I_{F3}(y_n)+\mathrm{i}(y_m+y_n)(y_m I_{F3}(y_m)$$
$$+y_n I_{F3}(y_n)-2\pi^{\frac{1}{2}}\mathrm{e}^{-\mathrm{i}\pi/4})]+O(N^{-\frac{3}{2}}), \tag{3.62}$$

where

$$C_{\mathrm{dsd}} = \frac{4\,\mathrm{e}^{-\mathrm{i}\pi/4}\,\mathrm{e}^{\mathrm{i}N(1-K_m\cos\theta_{\mathrm{c}}-K_n\sin\theta_{\mathrm{c}})}K_m^2K_n^2}{\pi^{\frac{3}{2}}\cos^3\theta_{\mathrm{c}}\sin^3\theta_{\mathrm{c}}(\cos\theta_{\mathrm{c}}+K_m)^2(\sin\theta_{\mathrm{c}}+K_n)^2}. \tag{3.63}$$

This expression for Z_{sd} is analytic at $y_m = -y_n$, but contains discontinuities at $y_m = 0, y_n = 0$. As long as $y_m + y_n \sim O(1)$ or larger at these points, the discontinuities cancel those in the oscillatory terms $\epsilon_m Z_{mo}$ and $\epsilon_n Z_{no}$, showing that the use of (3.13) for I_{nn2} and the neglect of the $C_{3\mathrm{b}}$ integral are valid in this case, even for $|y_n| \ll 1$. (The reason for this will become apparent in the following analysis.) However, if $y_m + y_n \sim O(N^{-\frac{1}{2}})$, the discontinuities in $\epsilon_m Z_{mo}$ and $\epsilon_n Z_{no}$ differ from those in (3.62) and the steepest descent integral must be re-examined. We now write

$$Z_{\mathrm{sd}} \sim Z_{\mathrm{sd}}^{\mathrm{o}} + Z_{\mathrm{sd}}^{\mathrm{i}} - \frac{4K_m^2K_n^2}{\pi^2\mu\eta}(1-\delta_n)\int_{C_{3\mathrm{b}}}\frac{\mathrm{e}^{\mathrm{i}\mu(K_z-K_m)}}{(K_z^2-K_m^2)^2}I_{nn1}(K_z)\,\mathrm{d}K_z, \tag{3.64}$$

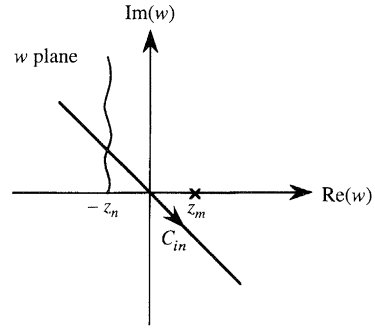

Figure 7. The w plane, with pole, branch cut and integration contour. The contour is deformed downwards for $z_n < 0$, and upwards onto the branch cut for $z_n > 0$.

where $Z^{\mathrm{o}}_{\mathrm{sd}}$ is the integral evaluated above, and

$$Z^{\mathrm{i}}_{\mathrm{sd}} = \frac{4K_m^2 K_n^2}{\pi^2 \mu\eta} \int_{C_{in}} \frac{\mathrm{e}^{\mathrm{i}\mu(K_z - K_m)}}{(K_z^2 - K_m^2)^2} (I^{\mathrm{i}}_{nn2} - I^{\mathrm{o}}_{nn2})\, \mathrm{d}K_z. \tag{3.65}$$

Here I^{o}_{nn2} and I^{i}_{nn2} are the leading-order terms of the non-uniform and transition expressions for I_{nn2} (equations (3.13) and (3.14)), and C_{in} is the region of the steepest descent contour where the transition expression for I_{nn2} applies. On making the substitutions $K_m = \cos\theta_{\mathrm{c}} + z_m/\mu$, $K_n = \sin\theta_{\mathrm{c}} + z_n/\eta$, $K_z = \cos\theta_{\mathrm{c}} + w/\mu$, the integration region is transformed to the w plane (figure 7) and C_{in} may be taken to cover the range $|w| < N^{\frac{1}{4}}$. Then (Graham 1993) the integration contour may be completed at 'infinity' with an error $O(N^{-\frac{1}{2}})$ at most, negligible here. For $z_n < 0$, the contour is deformed downwards, picking up a pole contribution for $z_m < 0$, and nothing for $z_m > 0$. When $z_n > 0$, it is deformed upwards onto the branch cut, picking up a pole contribution if $z_m > 0$. In the first two cases, the $C_{3\mathrm{b}}$ integral does not contribute and the addition to $Z^{\mathrm{o}}_{\mathrm{sd}}$ is entirely determined by the position of the z_m pole. This also turns out to be the case for $z_n > 0$, as the $C_{3\mathrm{b}}$ integral is found to cancel (to leading order) with the $Z^{\mathrm{i}}_{\mathrm{sd}}$ branch cut integral, leaving only the (potential) pole contribution. The result for Z_{sd} is thus

$$Z_{\mathrm{sd}} \sim Z^{\mathrm{o}}_{\mathrm{sd}} - (\epsilon_m + \epsilon_n - 1)\, C_{dz} N^{\frac{1}{2}} I_{FD}(z_m + z_n), \tag{3.66}$$

where

$$C_{dz} = \frac{2^{\frac{7}{2}} \mathrm{e}^{-\mathrm{i}\pi/4} K_m^2 K_n^2}{\pi^{\frac{1}{2}} (\cos\theta_{\mathrm{c}} + K_m)^2 (\sin\theta_{\mathrm{c}} + K_n)^2} \tag{3.67}$$

and

$$I_{FD}(z) = \left[\left(2 + \frac{2\mathrm{i}}{z} - \frac{3}{2z^2}\right)\left\{\frac{F^*(z^{\frac{1}{2}})}{z^{\frac{1}{2}}} - \frac{\pi^{\frac{1}{2}} \mathrm{e}^{-\mathrm{i}\pi/4}}{2z^{\frac{1}{2}}}\right\} - \frac{\mathrm{i}\mathrm{e}^{-\mathrm{i}z}}{z} + \frac{3\mathrm{e}^{-\mathrm{i}z}}{2z^2} + \frac{2\mathrm{i}\mathrm{e}^{-\mathrm{i}z}}{z^3}\right]. \tag{3.68}$$

The discontinuities in the additional term at $K_m = \cos\theta_{\mathrm{c}}$, $K_n = \sin\theta_{\mathrm{c}}$, are (to leading order) those required to cancel the discontinuities in the terms $Z^{\mathrm{o}}_{\mathrm{sd}}$, $\epsilon_m Z_{mo}$ and $\epsilon_n Z_{no}$. Thus, in this region it provides a smooth transition through the points $K_m = \cos\theta_{\mathrm{c}}$, $K_n = \sin\theta_{\mathrm{c}}$, whereas for z_m, z_n large (3.17) may be used to show that it becomes negligibly small.

(iii) *Singly-cross case*

In this case we consider the partial impedance, J^{x}_{mn}, defined by (3.4) and (3.5). The analysis proceeds exactly as for the direct case, with the exception that the symmetry arguments used to derive the transition forms of Z_{n1} are not applicable

here, so the corresponding terms are found instead by reversing the order of integration and proceeding as for Z_{m1}. Graham (1993) gives further details; the results may be summarized as

$$J^{\mathrm{x}}_{mn} = J^{\mathrm{x}}_{\mathrm{ex}} + \epsilon_m J^{\mathrm{x}}_{m\mathrm{o}} + \epsilon_n J^{\mathrm{x}}_{n\mathrm{o}} + J^{\mathrm{x}}_{m1} + J^{\mathrm{x}}_{n1} + J^{\mathrm{x}}_{\mathrm{sd}}. \tag{3.69}$$

The component terms correspond to those for the direct case, and take the following forms:

$$J^{\mathrm{x}}_{\mathrm{ex}} = -\frac{4\mathrm{i}}{\pi K_m Q\mu}\arctan\left(\frac{K_m}{Q}\right) + \frac{4}{\pi K_n P^2\mu\eta}\left[\frac{K_n}{1-K_n^2} + \frac{(K_n^2+P^2)}{K_m Q}\arctan\left(\frac{K_m K_n}{Q}\right)\right], \quad P^2 < 0, Q = \mathrm{i}P, \tag{3.70a}$$

$$J^{\mathrm{x}}_{\mathrm{ex}} = \frac{2\mathrm{i}}{\pi K_m P\mu}\left[\ln\left|\frac{K_m+P}{K_m-P}\right| + \epsilon_{1n}\,\mathrm{i}\pi\right] + \frac{4}{\pi K_n P^2\mu\eta}\left[\frac{K_n}{1-K_n^2} - \frac{(K_n^2+P^2)}{2K_m P}\left\{\ln\left|\frac{K_m K_n+P}{K_m K_n-P}\right| + (\epsilon_{1m}+\epsilon_{1n}-1)\,\mathrm{i}\pi\right\}\right], \quad P^2 > 0, \tag{3.70b}$$

$$J^{\mathrm{x}}_{m\mathrm{o}} \sim 2^{\frac{5}{2}}\mathrm{e}^{\mathrm{i}\pi/4}\,\mathrm{e}^{\mathrm{i}\eta[L_m-K_n]}K_n^2/\pi^{\frac{1}{2}}L_m^{\frac{1}{2}}K_m P^4\mu\eta^{\frac{3}{2}}, \tag{3.71}$$

$$J^{\mathrm{x}}_{n\mathrm{o}} \sim 2^{\frac{3}{2}}\mathrm{e}^{-\mathrm{i}\pi/4}\,\mathrm{e}^{\mathrm{i}\mu[L_n-K_m]}(1-r_1)/\pi^{\frac{1}{2}}L_n^{\frac{1}{2}}P^2\mu^{\frac{3}{2}} + O(N^{-\frac{5}{2}}), \tag{3.72}$$

except around coincidence ($P^2 \approx 0$), when

$$J^{\mathrm{x}}_{m\mathrm{o}} \sim -\frac{2^{\frac{5}{2}}\mathrm{e}^{\mathrm{i}\pi/4}K_n^2\,\eta^{\frac{1}{2}}}{\pi^{\frac{1}{2}}L_m^{\frac{1}{2}}K_m(K_n+L_m)^2\mu}\left[\left(2+\frac{\mathrm{i}}{z_2}\right)\left(\frac{F^*(z_2^{\frac{1}{2}})}{z_2^{\frac{1}{2}}} - \frac{\pi^{\frac{1}{2}}\mathrm{e}^{-\mathrm{i}\pi/4}}{2z_2^{\frac{3}{2}}}\right) - \frac{\mathrm{i}\mathrm{e}^{-\mathrm{i}z_2}}{z_2}\right] + O(N^{-\frac{3}{2}}), \tag{3.73}$$

$$J^{\mathrm{x}}_{n\mathrm{o}} \sim -\frac{2^{\frac{3}{2}}\mathrm{e}^{\mathrm{i}\pi/4}}{\pi^{\frac{1}{2}}L_n^{\frac{1}{2}}(K_m+L_n)\mu^{\frac{1}{2}}}\left[\left(2+\frac{\mathrm{i}r_1}{z_1}\right)\left(\frac{F^*(z_1^{\frac{1}{2}})}{z_1^{\frac{1}{2}}} - \frac{\pi^{\frac{1}{2}}\mathrm{e}^{-\mathrm{i}\pi/4}}{2z_1^{\frac{3}{2}}}\right) - \frac{\mathrm{i}r_1\mathrm{e}^{-\mathrm{i}z_1}}{z_1}\right] + O(N^{-\frac{3}{2}}), \tag{3.74}$$

$J^{\mathrm{x}}_{m1} \sim O(N^{-3})$, unless K_m is near one, when

$$J^{\mathrm{x}}_{m1} \sim -[8/\pi K_n^2(1+K_m)\mu\eta]\,F_{\mathrm{cs}}(x_m) + O(N^{-3}), \tag{3.75}$$

or K_n is close to zero, for which case

$$J^{\mathrm{x}}_{m1} \sim \frac{4\,\mathrm{e}^{\mathrm{i}\mu(1-K_m)}}{\pi(1-K_m^2)\mu\eta}\left[1 - \frac{\mathrm{e}^{-\mathrm{i}\pi/4}(1+2\mathrm{i}v_n^2)}{2\pi^{\frac{1}{2}}v_n}I_{F3}(v_n)\right] + O(N^{-3}). \tag{3.76}$$

Similarly, $J^{\mathrm{x}}_{n1} \sim O(N^{-3})$, except that, for $K_n \approx 1$,

$$J^{\mathrm{x}}_{n1} \sim \frac{8K_n^2}{\pi K_m^2(1+K_n)^2\mu}\left[\left(\mathrm{i}F_{\mathrm{cs}}(x_n) + \frac{\mathrm{e}^{-\mathrm{i}x_n}}{x_n}\right) - \frac{1}{\eta}\left(\frac{1}{K_m^2} + \frac{2}{1+K_n}\right)[(1+\mathrm{i}x_n)F_{\mathrm{cs}}(x_n) + \mathrm{e}^{-\mathrm{i}x_n}]\right] + O(N^{-3}), \tag{3.77}$$

and, for K_m near zero,

$$J^{\mathrm{x}}_{n1} \sim [4\,\mathrm{e}^{-\mathrm{i}\pi/4}\,\mathrm{e}^{\mathrm{i}\eta(1-K_n)}K_n^2/\pi^{\frac{3}{2}}v_m(1-K_n^2)^2\mu\eta]\,I_{F3}(v_m) + O(N^{-3}). \tag{3.78}$$

Lastly, $J^{\mathrm{x}}_{\mathrm{sd}} \sim O(N^{-3})$ except around $K_m \approx \cos\theta_{\mathrm{c}}$ or $K_n \approx \sin\theta_{\mathrm{c}}$, when

$$J^{\mathrm{x}}_{\mathrm{sd}} \sim J^{\mathrm{xo}}_{\mathrm{sd}} + (\epsilon_m+\epsilon_n-1)\,C_{xz}N^{-\frac{1}{2}}I_{FX}(z_m+z_n), \tag{3.79}$$

where

$$J_{\rm sd}^{\rm xo} \sim \frac{C_{\rm xsd}}{(y_m+y_n)^2 N^{\frac{3}{2}}}[I_{F3}(y_m)+I_{F3}(y_n)+2{\rm i}(y_m+y_n)(y_n I_{F3}(y_n)-\pi^{\frac{1}{2}}{\rm e}^{-{\rm i}\pi/4})]+O(N^{-2}), \tag{3.80}$$

with
$$C_{\rm xsd} = -\frac{2^{\frac{3}{2}}{\rm e}^{-{\rm i}\pi/4}\,{\rm e}^{{\rm i}N(1-K_m\cos\theta_{\rm c}-K_n\sin\theta_{\rm c})}K_n^2}{\pi^{\frac{3}{2}}\cos^3\theta_{\rm c}\sin^2\theta_{\rm c}(\cos\theta_{\rm c}+K_m)(\sin\theta_{\rm c}+K_n)^2} \tag{3.81}$$

and
$$C_{{\rm x}z} = \frac{2^{\frac{7}{2}}{\rm e}^{{\rm i}\pi/4}K_n^2}{\pi^{\frac{1}{2}}\cos\theta_{\rm c}(\cos\theta_{\rm c}+K_m)(\sin\theta_{\rm c}+K_n)^2}, \tag{3.82}$$

$$I_{FX}(z) = \left(2+\frac{\rm i}{z}\right)\left\{\frac{F^*(z^{\frac{1}{2}})}{z^{\frac{1}{2}}}-\frac{\pi^{\frac{1}{2}}{\rm e}^{-{\rm i}\pi/4}}{2z^{\frac{1}{2}}}\right\}-\frac{{\rm i}{\rm e}^{-{\rm i}z}}{z}+\frac{{\rm e}^{-{\rm i}z}}{z^2}. \tag{3.83}$$

(iv) *Doubly-cross case*

Here the quantity to be evaluated is the partial impedance $J_{mn}^{\rm xx}$, defined by (3.7) and (3.8), and the results are summarized by

$$J_{mn}^{\rm xx} = J_{\rm ex}^{\rm xx}+\epsilon_m J_{mo}^{\rm xx}+\epsilon_n J_{no}^{\rm xx}+J_{m1}^{\rm xx}+J_{n1}^{\rm xx}+J_{\rm sd}^{\rm xx}, \tag{3.84}$$

$$J_{\rm ex}^{\rm xx} = -\frac{8}{\pi K_m K_n Q\mu\eta}\arctan\left(\frac{K_m K_n}{Q}\right), \quad P^2<0, Q={\rm i}P, \tag{3.85a}$$

$$J_{\rm ex}^{\rm xx} = \frac{4}{\pi K_m K_n P\mu\eta}\left[\ln\left|\frac{K_m K_n+P}{K_m K_n-P}\right|+(\epsilon_{1m}+\epsilon_{1n}-1)\,{\rm i}\pi\right], \quad P^2>0, \tag{3.85b}$$

$$J_{mo}^{\rm xx} \sim -2^{\frac{5}{2}}{\rm e}^{{\rm i}\pi/4}\,{\rm e}^{{\rm i}\eta[L_m-K_n]}/\pi^{\frac{1}{2}}L_m^{\frac{1}{2}}K_m P^2\mu\eta^{\frac{3}{2}}+O(N^{-\frac{7}{2}}), \tag{3.86}$$

$$J_{no}^{\rm xx} \sim -2^{\frac{5}{2}}{\rm e}^{{\rm i}\pi/4}\,{\rm e}^{{\rm i}\mu[L_n-K_m]}/\pi^{\frac{1}{2}}L_n^{\frac{1}{2}}K_n P^2\mu^{\frac{3}{2}}\eta+O(N^{-\frac{7}{2}}), \tag{3.87}$$

unless $P^2\approx 0$ (coincidence), when

$$J_{mo}^{\rm xx} \sim -\frac{2^{\frac{7}{2}}{\rm e}^{-{\rm i}\pi/4}}{\pi^{\frac{1}{2}}L_m^{\frac{1}{2}}K_m(K_n+L_m)\mu\eta^{\frac{1}{2}}}\left[\frac{F^*(z_2^{\frac{1}{2}})}{z_2^{\frac{1}{2}}}-\frac{\pi^{\frac{1}{2}}{\rm e}^{-{\rm i}\pi/4}}{2z_2^{\frac{1}{2}}}\right]+O(N^{-\frac{5}{2}}), \tag{3.88}$$

$$J_{no}^{\rm xx} \sim -\frac{2^{\frac{7}{2}}{\rm e}^{-{\rm i}\pi/4}}{\pi^{\frac{1}{2}}L_n^{\frac{1}{2}}K_n(K_m+L_n)\mu^{\frac{1}{2}}\eta}\left[\frac{F^*(z_1^{\frac{1}{2}})}{z_1^{\frac{1}{2}}}-\frac{\pi^{\frac{1}{2}}{\rm e}^{-{\rm i}\pi/4}}{2z_1^{\frac{1}{2}}}\right]+O(N^{-\frac{5}{2}}), \tag{3.89}$$

$J_{m1}^{\rm xx} \sim O(N^{-3})$, with exceptions

$$J_{m1}^{\rm xx} \sim [8/\pi K_n^2(1+K_m)\mu\eta]F_{\rm cs}(x_m)+O(N^{-3}), \quad K_m\approx 1, \tag{3.90}$$

and
$$J_{m1}^{\rm xx} \sim [4\,{\rm e}^{-{\rm i}\pi/4}\,{\rm e}^{{\rm i}\mu(1-K_m)}/\pi^{\frac{3}{2}}v_n(1-K_m^2)\mu\eta]I_{F3}(v_n)+O(N^{-3}), \quad K_n\approx 0. \tag{3.91}$$

Similarly, the significant $J_{n1}^{\rm xx}$ contributions are

$$J_{n1}^{\rm xx} \sim [8/\pi K_m^2(1+K_n)\mu\eta]F_{\rm cs}(x_n)+O(N^{-3}), \quad K_n\approx 1, \tag{3.92}$$

and
$$J_{n1}^{\rm xx} \sim [4\,{\rm e}^{-{\rm i}\pi/4}\,{\rm e}^{{\rm i}\eta(1-K_n)}/\pi^{\frac{3}{2}}v_m(1-K_n^2)\mu\eta]I_{F3}(v_m)+O(N^{-3}), \quad K_m\approx 0. \tag{3.93}$$

Finally, $J_{\rm sd}^{\rm xx} \sim O(N^{-3})$ away from the regions $K_m\approx\cos\theta_{\rm c}$, $K_n\approx\sin\theta_{\rm c}$, in which it becomes

$$J_{\rm sd}^{\rm xx} \sim J_{\rm sd}^{\rm xxo}+(\epsilon_m+\epsilon_n-1)\,C_{{\rm x}xz}N^{-\frac{3}{2}}I_{FXX}(z_m+z_n), \tag{3.94}$$

where
$$J_{\rm sd}^{\rm xxo} \sim [C_{\rm xxsd}/(y_m+y_n)N^2][I_{F3}(y_m)+I_{F3}(y_n)]+O(N^{-\frac{5}{2}}), \tag{3.95}$$

with $$C_{\mathrm{xxsd}} = \frac{4\,\mathrm{e}^{-\mathrm{i}\pi/4}\,\mathrm{e}^{\mathrm{i}N(1-K_m\cos\theta_\mathrm{c}-K_n\sin\theta_\mathrm{c})}}{\pi^{\frac{3}{2}}\cos^2\theta_\mathrm{c}\sin^2\theta_\mathrm{c}(\cos\theta_\mathrm{c}+K_m)(\sin\theta_\mathrm{c}+K_n)} \tag{3.96}$$

and $$C_{\mathrm{xxz}} = 2^{\frac{9}{2}}\mathrm{e}^{-\mathrm{i}\pi/4}/[\pi^{\frac{1}{2}}\cos\theta_\mathrm{c}\sin\theta_\mathrm{c}(\cos\theta_\mathrm{c}+K_m)(\sin\theta_\mathrm{c}+K_n)], \tag{3.97}$$

$$I_{FXX}(z) = \frac{F^*(z^{\frac{1}{2}})}{z^{\frac{1}{2}}} - \frac{\pi^{\frac{1}{2}}\mathrm{e}^{-\mathrm{i}\pi/4}}{2z^{\frac{1}{2}}} - \frac{\mathrm{i}\mathrm{e}^{-\mathrm{i}z}}{2z}. \tag{3.98}$$

(*e*) *Results summary and validation*

(i) *Summary of asymptotic results*

The analysis presented in §§3*b–d* yields asymptotic expressions for the impedance integral, Z^{0f}_{mnpq}, in terms of the dimensionless modal wavenumbers $K_m = k_m/k_0$, $K_n = k_n/k_0$, (with K_p and K_q defined similarly) and the (large) dimensionless plate length, breadth and diagonal $\mu = k_0 a$, $\eta = k_0 b$, $N = (\mu^2+\eta^2)^{\frac{1}{2}}$. In all the cases considered, the relevant integral is expressed as a sum of six terms, one exact (which usually gives the leading order contribution) and five evaluated asymptotically. Thus, for the direct case ($m = p, n = q$),

$$Z^{\mathrm{0f}}_{mnmn} = Z_{\mathrm{ex}} + \epsilon_m Z_{mo} + \epsilon_n Z_{no} + Z_{m1} + Z_{n1} + Z_{\mathrm{sd}}, \tag{3.99}$$

where ϵ_m is one for $K_m < \cos\theta_\mathrm{c}$, and zero otherwise, and ϵ_n is defined similarly in relation to $\sin\theta_\mathrm{c}$. The tangent of the angle θ_c is equal to the plate aspect ratio, b/a.

In (3.99), Z_{ex} is the exact term, and is given by (3.46)–(3.48), while Z_{mo} and Z_{no} are oscillatory terms, whose most general forms are defined by (3.50) and (3.52) respectively. The function $F^*(z)$ in these expressions is a Fresnel integral, given by (3.16). The next two terms, Z_{m1} and Z_{n1}, also form a pair, and are significant in two cases. Z_{m1} becomes important when K_m is around one ((3.54), (3.55)) or K_n near zero ((3.57), (3.58)) and Z_{n1} is similarly relevant for K_n close to one or K_m to zero ((3.60), (3.61)). Finally, Z_{sd} contributes when K_m is near $\cos\theta_\mathrm{c}$, or K_n near $\sin\theta_\mathrm{c}$, and is given by (3.62) and (3.63), with modifications described by (3.66)–(3.68) if both transitions occur very nearly at the same time.

These expressions combine to specify Z^{0f}_{mnmn} to an accuracy $O(N^{-2})$, apart from around coincidence ($K_m^2+K_n^2 \approx 1$), where it is $O(N^{\frac{1}{2}})$ and the following term, of $O(N^{-\frac{1}{2}})$, has not been found. They also contain all the formulae given by Leppington *et al.* (1982) for the real part of the impedance, and the leading order below coincidence ($K_m^2+K_n^2 > 1$) imaginary term noted by Davies (1971*a*) and Chang & Leehey (1979). The unified approach presented here has thus reproduced and extended the known expressions for $\mathrm{Re}\,(Z^{\mathrm{0f}}_{mnmn})$, while simultaneously obtaining, for the first time, a full description of $\mathrm{Im}\,(Z^{\mathrm{0f}}_{mnmn})$ over the entire parameter range.

For the singly-cross case ($m \neq p, n = q$) the impedance is written in the form

$$Z^{\mathrm{0f}}_{mnpn} = \{K_m K_p/[(K_p^2-K_m^2)]\}[J^{\mathrm{x}}_{pn} - J^{\mathrm{x}}_{mn}], \tag{3.100}$$

and the analysis for the partial impedance then yields six component terms ((3.69)–(3.83)) analogous to those of (3.99). These expressions, like those for the direct case, are accurate to $O(N^{-2})$ except around coincidence, where the leading term is $O(N^{-\frac{1}{2}})$ and the following, $O(N^{-\frac{3}{2}})$, term has not been found. They are also entirely new, none of them having been given by previous authors.

Symmetry arguments may be exploited to obtain the appropriate expressions for the $m = p, n \neq q$ case (given by the formulae for $m \neq p$, $n = q$ with K_m, K_n and μ, η

PHILOSOPHICAL TRANSACTIONS OF THE ROYAL SOCIETY A MATHEMATICAL, PHYSICAL & ENGINEERING SCIENCES

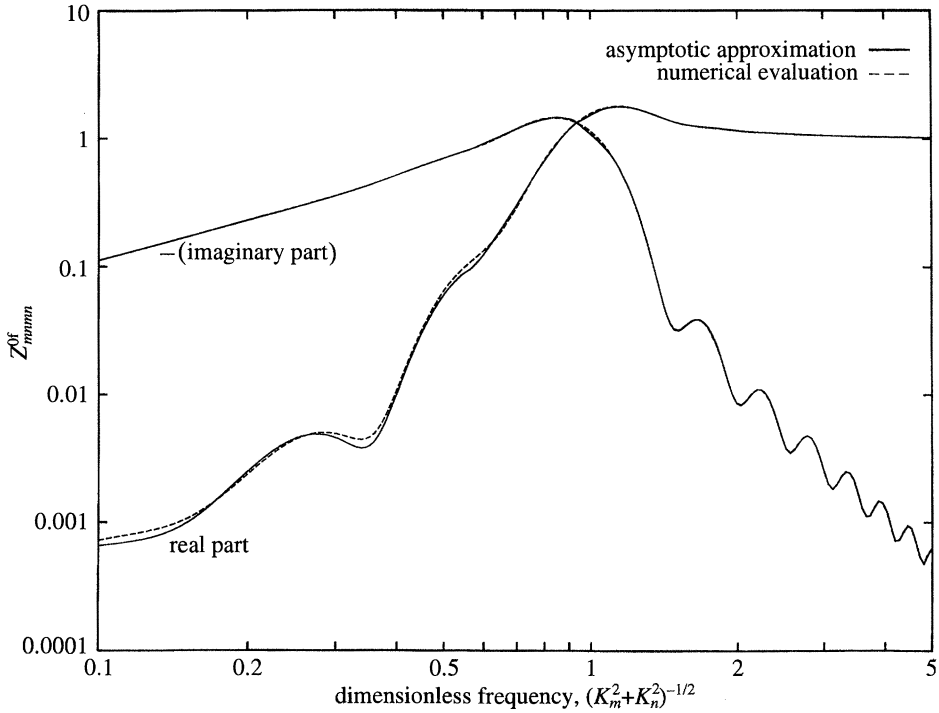

Figure 8. Numerical and asymptotic results for the direct impedance: $(m, n) = (5, 3)$, $a = 1.34$ m, $b = 0.50$ m. The dimensionless frequency is one when the modal and acoustic wavelengths are equal (coincidence). Above this frequency, the mode is an efficient radiator ($\mathrm{Re}\,(Z^{0f}_{mnmn}) \approx 1$).

interchanged), so it only remains to consider the doubly-cross case ($m \neq p, n \neq q$), where the impedance takes the form

$$Z^{0f}_{mnpq} = [K_m K_n K_p K_q/(K_p^2 - K_m^2)(K_q^2 - K_n^2)][J^{xx}_{pq} - J^{xx}_{mq} - J^{xx}_{pn} + J^{xx}_{mn}], \quad (3.101)$$

with partial impedance components defined by (3.84)–(3.98). These formulae specify J^{xx}_{mn} to an accuracy $O(N^{-\frac{5}{2}})$ usually, $O(N^{-\frac{3}{2}})$ around coincidence, and, like the expressions for J^{x}_{mn}, they are entirely new.

Most of the results presented here require validation, as only those for the direct impedance can be checked (partially) against existing theory. Thus in the following section we compare the asymptotic approximations with numerical evaluations of the relevant integrals.

(ii) *Comparison of numerical and asymptotic results*

Numerical evaluation of the integrals Z^{0f}_{mnmn}, J^{x}_{mn}, and J^{xx}_{mn} is performed with standard routines from the NAG library, with asymptotic corrections to reduce the errors associated with the truncation of the infinite integration range. For the partial impedances, where significant cancellation occurs, the range is split at the point where the integrand changes sign, with a corresponding improvement in speed and robustness at a (potential) cost in accuracy.

The asymptotic results are implemented in the formulation presented in (3.99). This presents problems in the transition regions, where pairs of terms have matching singularities of opposite sign, and the difference between two large numbers is

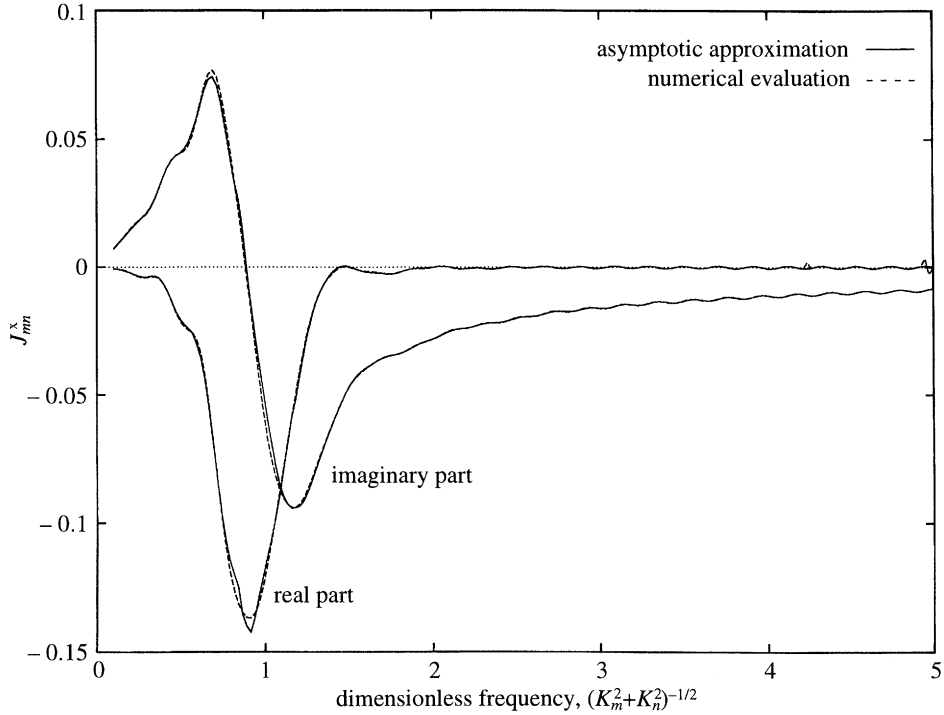

Figure 9. Numerical and asymptotic results for the singly-cross partial impedance: $(m, n) = (5, 3)$, $a = 1.34$ m, $b = 0.50$ m. The asymptotics fare least well around coincidence, where approximate terms are most significant. Note also the computational inaccuracies at high frequencies, where numerical evaluation of J^{x}_{mn} becomes difficult.

required. (In the Z^{0f}_{mnmn} and J^{x}_{mn} transition regions, the difficulty is exacerbated, as the asymptotic terms are not known to an accuracy sufficient to cancel the lower-order singularities in Z_{ex} and J^{x}_{ex}.) Linear interpolation is used to avoid the errors associated with direct evaluation close to such points.

Numerical and asymptotic evaluations of Z^{0f}_{mnmn}, J^{x}_{mn} and J^{xx}_{mn} for the case $(m, n) = (5, 3)$, $a = 1.34$ m, $b = 0.50$ m, are shown in figures 8–10. The results are plotted against a dimensionless frequency, $(K_m^2+K_n^2)^{-\frac{1}{2}}$, which is one when the mode is at coincidence, a point that marks its transition from an inefficient ($\mathrm{Re}\,(Z^{0f}_{mnmn})$ small) to an efficient ($\mathrm{Re}\,(Z^{0f}_{mnmn})$ around one) radiator. For all three quantities the analytical approximations are clearly successful in representing the integral. Three other cases must be considered, to test the asymptotic formulae fully (Graham 1993); in each, agreement better than that shown here is found and the results may thus be accepted as valid.

Three interesting features emerge from figures 8–10. First, the agreement is good down to very low N, about 3 when the dimensionless frequency is 0.1. This is because the exact terms dominate here, and inaccuracies in the asymptotic terms are relatively unimportant. The worst agreement tends to be at higher N, around coincidence, where the asymptotic and exact terms are of equal (large) magnitude. Secondly, the problems in numerical evaluation of the integrals at high frequencies are illustrated by the computational errors evident in figure 9 when the result is small. In these regions the asymptotics are not only more efficient, but also more accurate. Finally, the plots bring out the difference in magnitude between the singly-

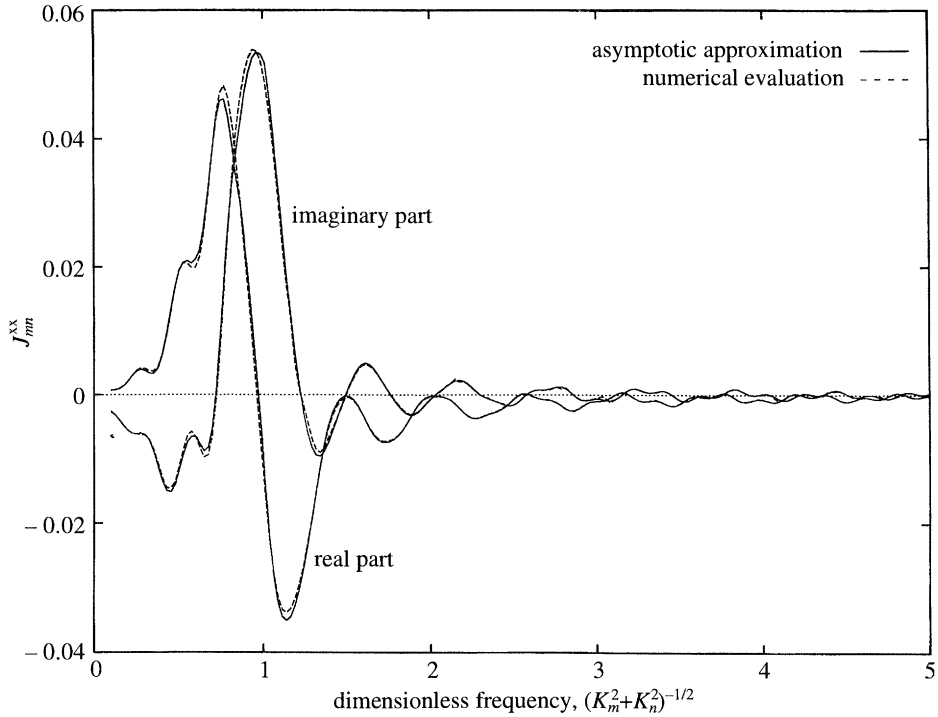

Figure 10. Numerical and asymptotic results for the doubly-cross partial impedance: $(m, n) = (5, 3)$, $a = 1.34$ m, $b = 0.50$ m. Note the reduced magnitude of the impedance compared with the singly-cross case (figure 9).

cross and doubly-cross impedances (typically $O(N^{-1})$ and $O(N^{-2})$ respectively). Modes sharing a common mode number are thus well coupled in comparison to the majority.

It remains to consider the regions of (K_m, K_n) parameter space not covered by the asymptotic approximations above. Analytical expressions for Z_{mo} and Z_{n1} with $K_m \approx 0$, $K_n \approx 1$ and for Z_{no} and Z_{m1} with $K_m \approx 1$, $K_n \approx 0$ have not been obtained, and there is a similar lack for the corresponding cross terms. This problem is resolved by a hybrid approach, where the asymptotic expressions found in §3*c* for the first integral are used to provide the integrand for a numerical evaluation of the second integral. The results (Graham 1993) show excellent agreement with fully numerical evaluations.

4. Plate vibration and radiation

(*a*) *Introduction*

The availability of asymptotic expressions for Z^{0f}_{mnpq} makes it possible to solve (2.4) in régimes involving many modes without neglecting coupling terms. As our aim is to assess the accuracy of the diagonal approximation in engineering situations, we wish to investigate a practical structure, rather than one that deliberately over-emphasizes the fluid-loading (cf. Davies 1971*b*). We thus consider the response of a steel plate (specified in table 1) to boundary-layer excitation in water ($\rho_0 = 1000$ kg m^{-3}, $c_0 = 1500$ m s^{-1}) over the frequency range 1–5 kHz.

In boundary-layer excitation problems involving water, flow Mach numbers are very low, so that the convective peak in the wavenumber–frequency spectrum is at

Table 1. *Fluid-loaded plate parameters*

length, a	2.0 m	thickness, h	0.025 m	mass/unit area, M	195 kg m^{-2}
breadth, b	1.5 m	bending stiffness, B_r	3.0×10^5 N m^{-2}	damping factor, ϵ_s	0.02

wavenumbers too high for significant structural response to occur. Instead, the structure responds at lower wavenumbers, and an approximate calculation indicates that this response is negligibly affected (via coupling) by that at the convective wavenumber. Additionally, Hwang & Maidanik (1990) have shown that the modal excitation terms Φ_{mnmn} are dominated by the contribution from the wavenumber–frequency spectrum at the modal wavenumbers, rather than at the convective wavenumber, so it is sufficient to consider only the low-wavenumber part of the excitation spectrum. This region is not yet well specified, but experimental evidence to date (Blake 1986) suggests that it is reasonably flat, and we shall take it to be of constant level Φ_c. This approximation neglects differences between the supersonic and (subsonic) low-wavenumber régimes, and also any local increase in the spectrum around the acoustic wavenumber. However, it has the virtue of simplicity and is a useful approach for investigating the effect of the coupling terms.

Having specified our numerical example, we now consider what to expect in the light of previous work. The diagonal approximation has been shown to be accurate when resonant modes are also efficient radiators (Leppington *et al.* 1986), a condition found above a certain critical frequency, which here exceeds 9160 Hz (the value calculated neglecting fluid-loading). We thus find ourselves in the potentially interesting region below the critical frequency where, according to Leppington *et al.* and Mkhitarov (1972), the effect of coupling is strongest for interactions between resonant modes. Mkhitarov's condition for this effect to be negligible, based on an iterative solution with the diagonal approximation as leading term, is complex, but an order of magnitude equivalent, $N\epsilon_s \gg \epsilon_{f0}$, may be found by putting d_{mn}, $d_{pq} \sim \epsilon_s$ (resonant, inefficient modes) and $Z^{0f}_{mnpq} \sim O(N^{-1})$, which is the largest value it can take if the (small) coincidence regions are neglected. At 1 kHz, we have $N\epsilon_s \approx 0.2$, $\epsilon_{f0} \approx 1.2$, so this condition is clearly not satisfied at the lower frequencies, and is only weakly true even at 5 kHz. Thus, given the presence of overlapping resonances in this example, we expect the coupling to have a significant effect. (Note that Mkhitarov's condition for appreciable resonance overlap, that $(a/b)^2$ be expressible as the ratio of two small integers, is too restrictive. Here it is not satisfied, but overlap still occurs and the results differ little from the case with $a = 2$ m, $b = 2^{\frac{1}{2}}$ m.)

When coupling is important, Leppington *et al.* predict that the diagonal approximation will still give an accurate result for the frequency-band-averaged radiation. This statement is contradicted by Davies (1971*b*), who notes that, if only one mode is driven, the other modes must absorb acoustic energy equal to their structural dissipation, and thus concludes that the effect of coupling will be to increase vibration and reduce radiation compared with the diagonal approximation. However, this argument is based on a mischaracterization of the coupling as direct only, and ignores its leaky aspect (see §2*c*(iii)), which may result in mutual radiation by a mode pair. Furthermore, Davies does not give a full treatment of the variation in input power, which might cause an increase in radiation in spite of an increased tendency towards vibration. His arguments thus remain to be confirmed, and will be reconsidered in the light of the numerical results presented here.

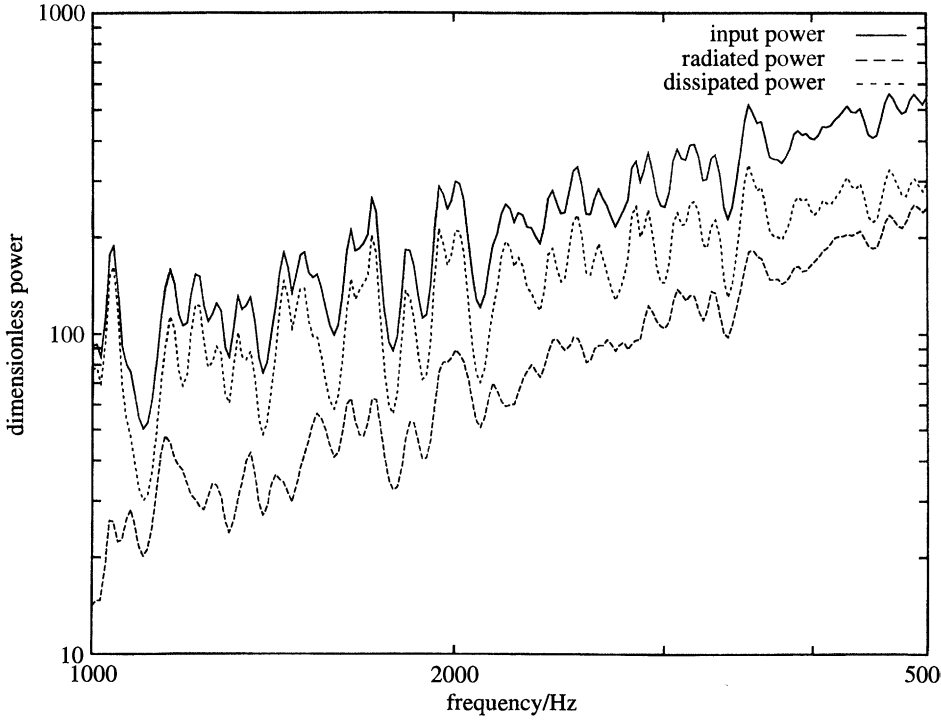

Figure 11. Dimensionless input ($M\omega S_t(\omega)/\Phi_c$), radiated ($M\omega S_0(\omega)/\Phi_c$) and dissipated ($M\omega S_d(\omega)/\Phi_c$) power spectra for the water-loaded plate. The low radiation efficiency in this frequency range is clearly evident.

(*b*) *Comparison of full and diagonal solutions*

(i) *Numerical implementation*

Given our flat wavenumber–frequency spectrum, the cross-modal excitation becomes $\Phi_{mnpq} = \Phi_c \delta_{mp} \delta_{nq}$, and (2.14), (2.16) and (2.17) reduce to a form where the only coupling arises from Y_{mnpq}. A further useful simplification is then obtained by non-dimensionalizing the spectra on $\Phi_c/M\omega$, and all results will be presented thus.

For the evaluation of the modal acoustic impedances the asymptotic results are entirely satisfactory unless N is small (< 17.5) at coincidence, or one of the dimensionless modal wavenumbers is near unity there. In these cases the evaluation is either fully numerical or hybrid, respectively, until the mode is some way above coincidence. A single-frequency comparison of the solution using this combined approach with that obtained completely numerically indicated error levels well below those associated with the diagonal approximation.

Finally, the matrix inversion is performed with a standard LU decomposition routine, with partial pivoting, adapted from an algorithm given by Press *et al.* (1989). This has been found to be both accurate and computationally efficient. The number of modes to include in the matrix is determined by using a truncation criterion based on the dimensionless impedance d_{mn}, and optimized by an investigation of its effect on the diagonal approximation solutions. All mass-limited and resonant modes are included, and stiffness-limited modes are ignored only when their contribution to the dissipated power (their most significant effect) is negligible.

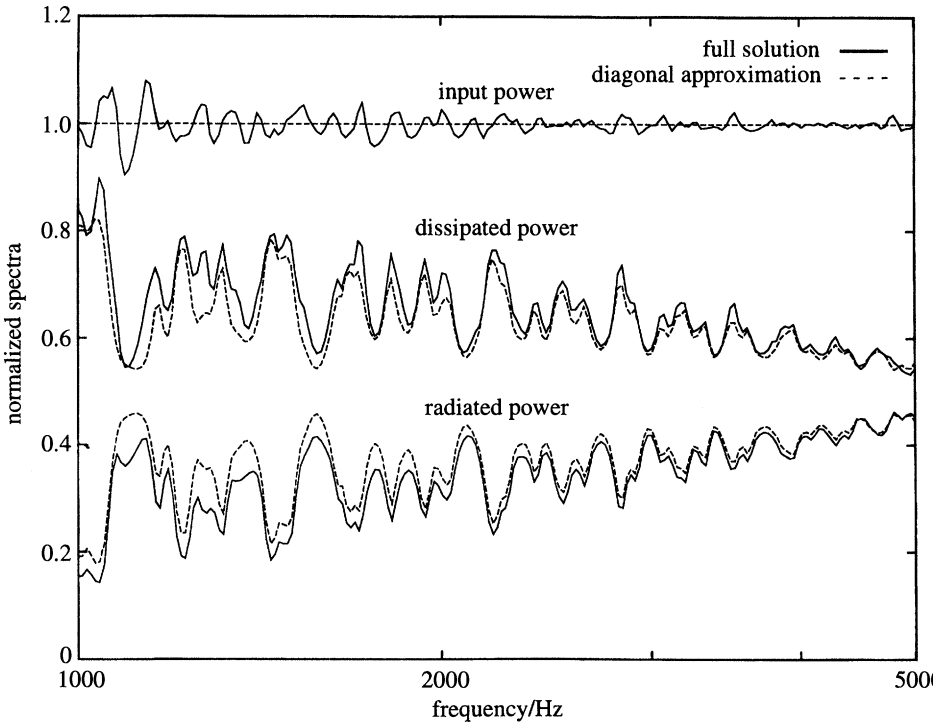

Figure 12. Comparison between full and diagonal solutions for the power spectra. The results are normalized on the diagonal approximation input power spectrum $S_t^d(\omega)$, and show that including coupling tends to increase vibration (dissipation) at the expense of radiation.

(ii) *Overall results*

The dimensionless input, radiated and dissipated power spectra for our plate are shown in figure 11. At the lower frequencies most of the input power is dissipated in the structure, but the proportion radiated increases with frequency, showing the effect of approaching the critical frequency. Rather similar results are obtained when coupling is neglected, and the two sets are best compared by normalizing all spectra on the diagonal approximation input power spectrum, $S_t^d(\omega)$ (figure 12). We see that the inclusion of coupling effects may result in either an increase or a decrease in input power, with no noticeable bias, but there is a clear tendency for plate vibration to increase at the expense of acoustic radiation. These results confirm some of the expectations mentioned in §4*a*, but the errors associated with the diagonal approximation are surprisingly small, suggesting that conditions for the neglect of coupling less stringent than $N\epsilon_s \gg \epsilon_{f0}$ may be found, given a better understanding of the problem. To this end, we first consider the contributions made by different classes of mode, and then investigate unimodal excitation.

(iii) *Results by mode class*

For this analysis the modes are classified into four types: efficient (class 1), mass-limited (class 2), resonant (class 3) and stiffness-limited (class 4). Any mode with $\mathrm{Re}\,(Z^{of}_{mnmn}) > 1$ is deemed efficient; in practice this entails all modes above coincidence and a few below, but close to, coincidence. Among the remainder, a mode is classed as resonant if the neglect of $\mathrm{Re}\,(d_{mn})$ would lead to an error of greater than 5% in calculating its response amplitude (under the diagonal approximation), and

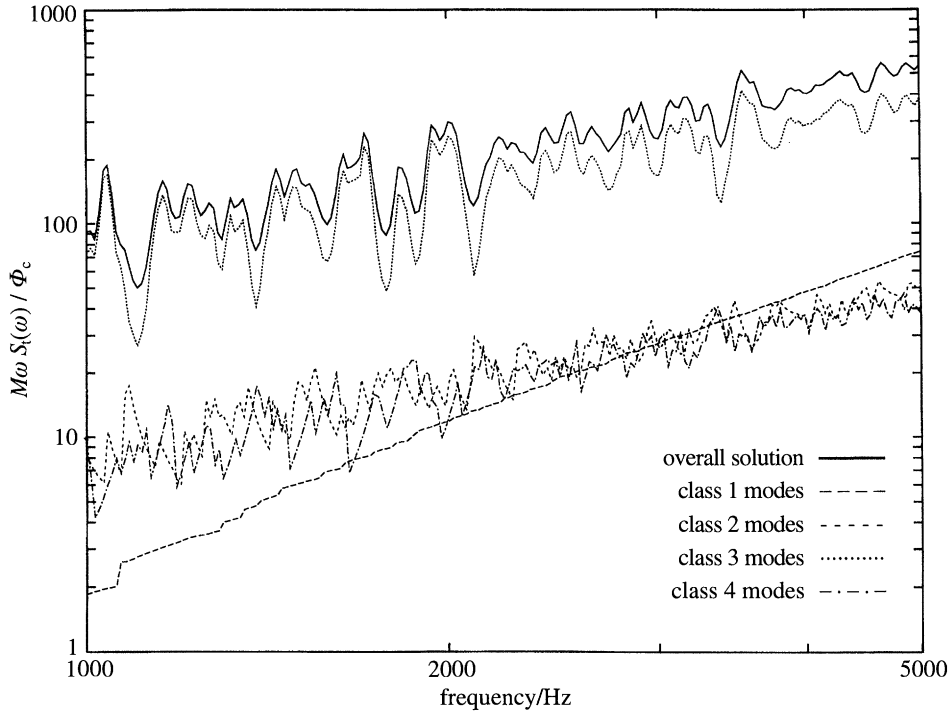

Figure 13. Dimensionless input power spectra by mode class. The overall solution is dominated by the input to the resonant modes.

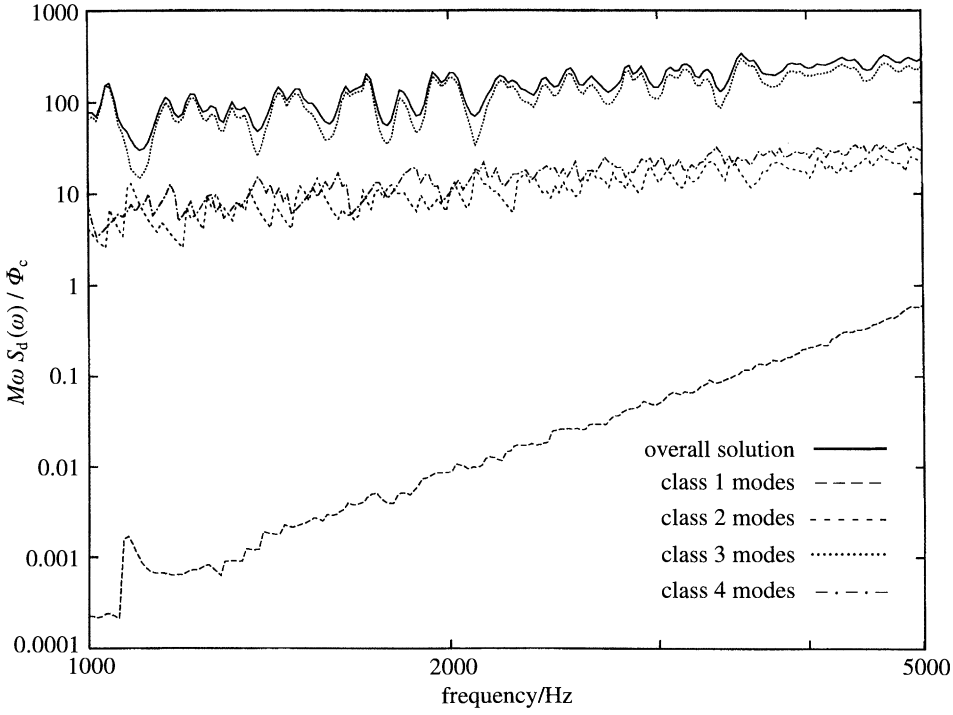

Figure 14. Dimensionless dissipated power spectra by mode class. Vibration levels are dominated by contributions from the resonant modes, and this is reflected in the dissipated power.

PHILOSOPHICAL TRANSACTIONS OF THE ROYAL SOCIETY A MATHEMATICAL, PHYSICAL & ENGINEERING SCIENCES

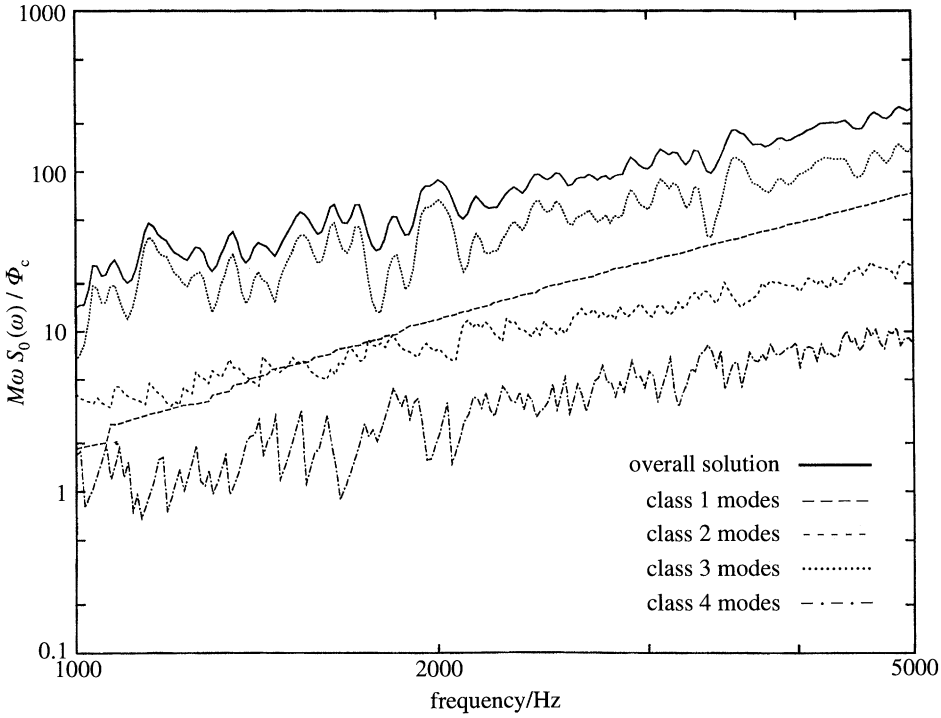

Figure 15. Dimensionless radiated power spectra by mode class. When compared with the dissipated power spectra of figure 14, the influence of radiation efficiency is clear.

the mass-limited and stiffness-limited classes contain the remaining above and below resonance modes respectively. The dimensionless input, dissipated and radiated power spectra for the four mode classes are shown, along with the respective overall spectra, in figures 13–15. Unsurprisingly, the input and dissipated powers are dominated by the resonant modes, but this is not so for the radiated power, where the efficient modes also make a significant contribution.

Again, comparison with the diagonal approximation is by normalized spectra. We find that the efficient modes (figure 16) show significant percentage changes in velocity when coupling is included, but their dissipation is so low that the effect on the input and radiated powers is negligible, and both are little altered from the diagonal approximation. The mass-limited modes (figure 17) show a different input power trend, the full solution being consistently below the diagonal approximation over most of the frequency range. This behaviour is repeated in the spectra for the radiated power, but not in those for the dissipated power, which are substantially the same. Moving on, the dominance of the resonant modes is confirmed by the resemblance between figure 18 and figure 12, described earlier. Here, though, we should additionally note that the variations in input power compared with the diagonal approximation, although unbiased, correlate well with the peaks and troughs of the input power spectrum. Finally, the stiffness-limited modes (figure 19) show similar characteristics to the mass-limited modes. The most significant difference is in the relative importance of dissipation and radiation, owing to the very low radiation efficiency of this class.

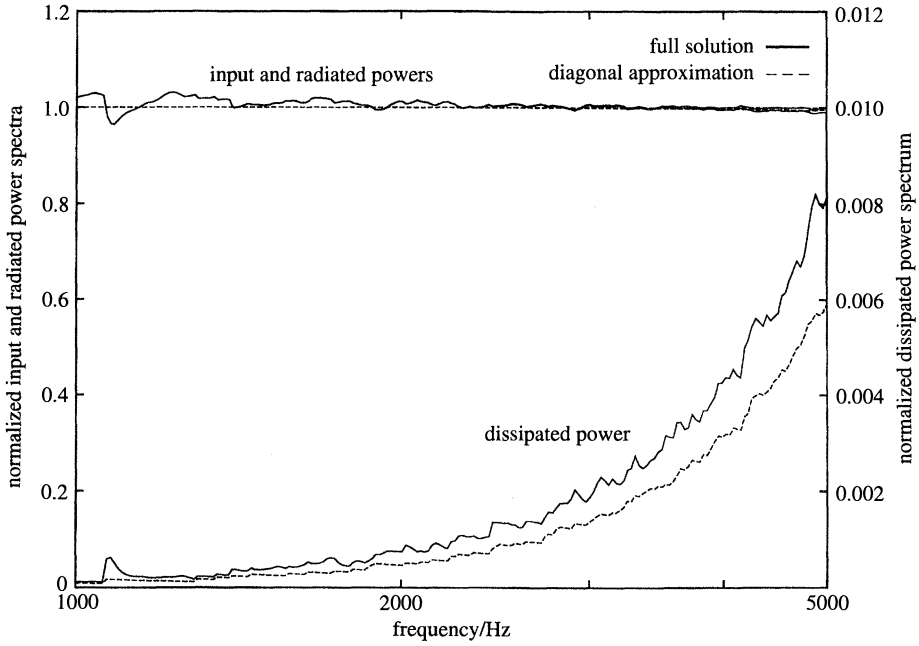

Figure 16. Class 1 modes: comparison between full and diagonal solutions for the power spectra. The results are normalized on the diagonal approximation input power spectrum for this class, and demonstrate the low vibration and dissipation levels of the efficient modes. The effect of coupling is small in absolute terms.

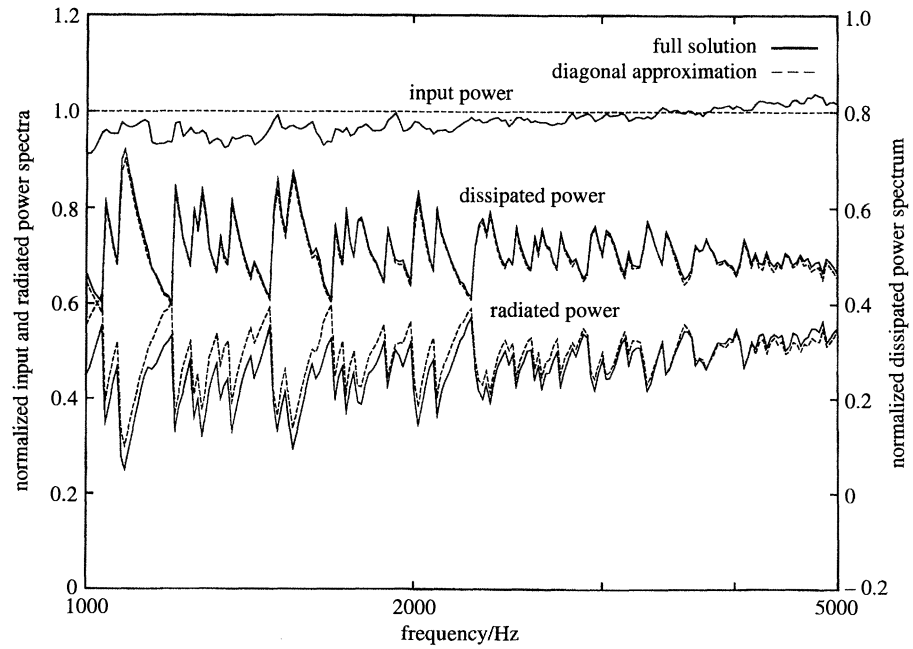

Figure 17. Class 2 modes: comparison between full and diagonal solutions for the power spectra. The effect of coupling is generally a reduction in input and radiated power, with little change in vibration levels.

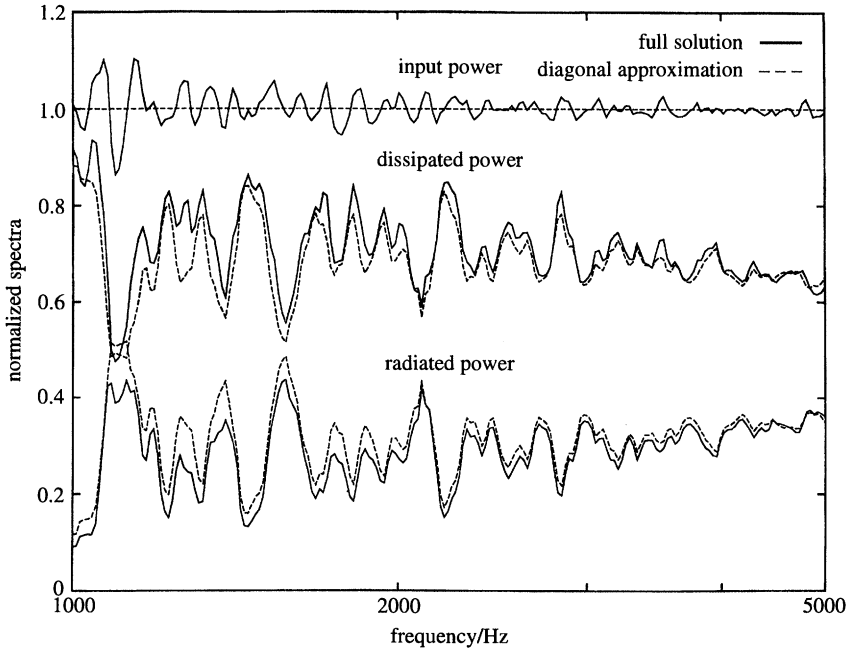

Figure 18. Class 3 modes: comparison between full and diagonal solutions for the power spectra. The inclusion of coupling results in increased vibration, decreased radiation, and an unbiased fluctuation in input power. The latter correlates with the peaks and troughs of the corresponding spectrum (figure 13).

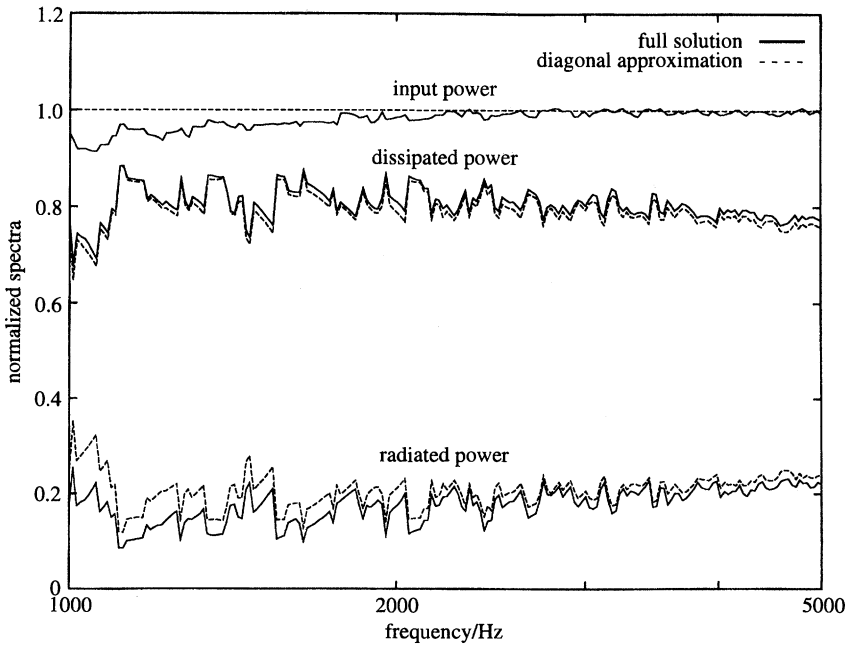

Figure 19. Class 4 modes: comparison between full and diagonal solutions for the power spectra. The coupling has an effect similar to that for class 2 modes. Note the very low radiation efficiency of these stiffness-limited modes.

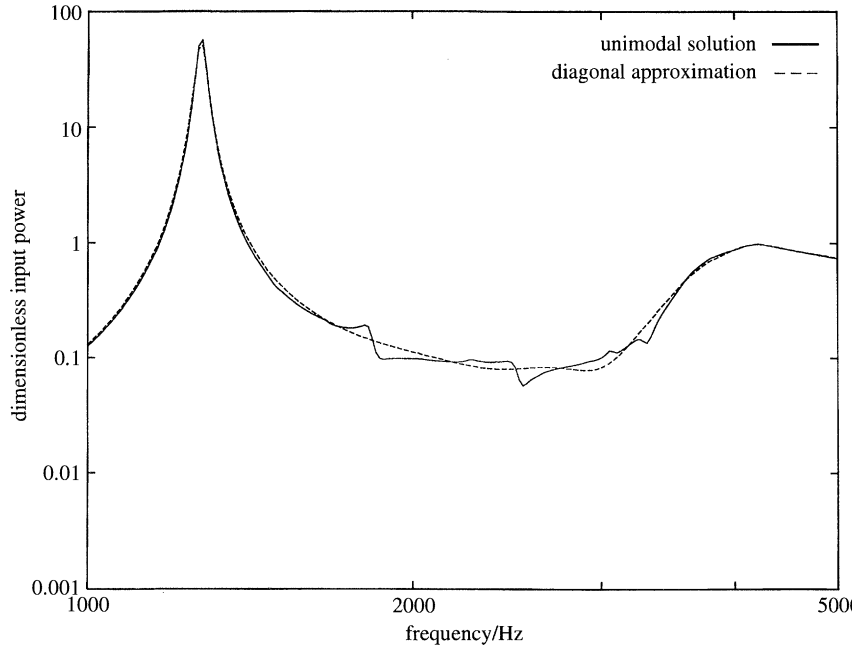

Figure 20. Dimensionless input power spectrum for mode (9, 3): unimodal ($M\omega S_{tmn}(\omega)/\Phi_c$) and diagonal ($M\omega S^d_{tmn}(\omega)/\Phi_c$) solutions. Here the result of including coupling is an increase around the resonance peak, a decrease either side and oscillations at resonance frequencies of modes well coupled to (9, 3).

(iv) *Unimodal excitation*

The trends observed in figures 16–19 may be understood by investigating the response of the system to single-mode driving. This is more than a useful *ad hoc* simplification: because our model forcing is uncoupled, the overall behaviour is in fact an exact superposition of all such unimodal excitation cases. A suitable mode to consider is (9, 3), which passes through all four classes over the 1–5 kHz frequency range. Its input power spectrum is shown, along with the diagonal approximation, in figure 20. At the resonance peak, the effect of including coupling is to cause a slight increase in input power, while on either side the reverse is true. Further above resonance, the full solution has single oscillations about the diagonal approximation at distinct points, which correspond to the resonance frequencies of modes well coupled to (9, 3): for example, the first such oscillation is at the resonance frequency of (11, 3). Finally, once (9, 3) becomes efficient, the unimodal and diagonal solutions coincide almost exactly. The solutions for radiated power are shown in figure 21, with the unimodal solution lower than the diagonal approximation in the region of resonance, then mirroring the input power behaviour above resonance and in the efficient region. Lastly, the solutions for dissipated power (figure 22) are remarkably similar everywhere, except at resonance, where the diagonal approximation is lower. Some variations on this behaviour occur among other modes. First, the oscillations seen in the input and radiated powers above resonance may sometimes also appear below resonance, and are occasionally biased to the positive or negative side of the diagonal solution. Secondly, not all modes show any noticeable difference in input power at resonance. Nonetheless, (9, 3) is representative of the general tendencies observed when unimodal excitation is considered.

PHILOSOPHICAL TRANSACTIONS OF THE ROYAL SOCIETY A MATHEMATICAL, PHYSICAL & ENGINEERING SCIENCES

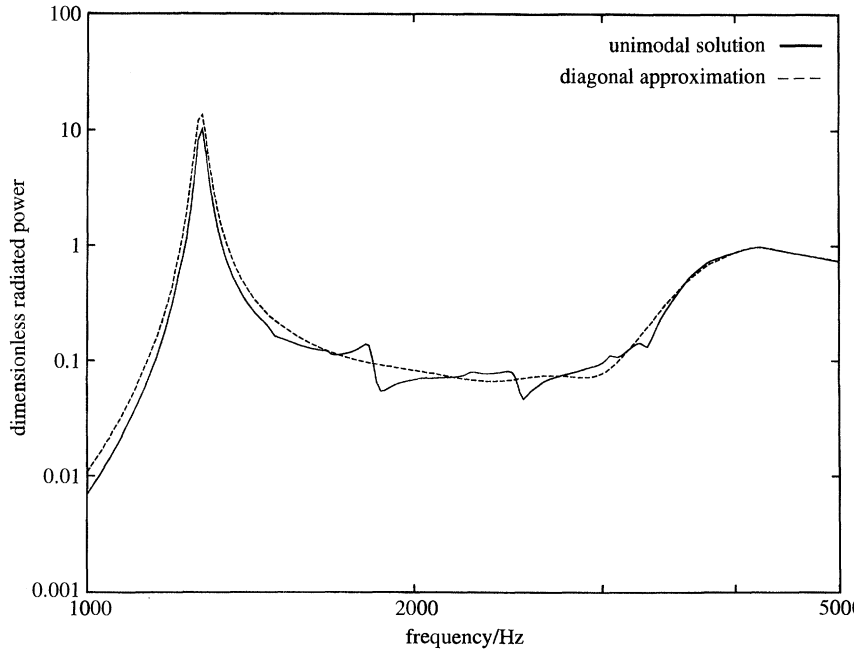

Figure 21. Dimensionless radiated power spectrum for mode (9, 3): unimodal ($M\omega S^{\mathrm{u}}_{0mn}(\omega)/\Phi_{\mathrm{c}}$) and diagonal ($M\omega S^{\mathrm{d}}_{0mn}(\omega)/\Phi_{\mathrm{c}}$) solutions. Around resonance, coupling lowers the unimodal solution, whereas elsewhere the behaviour is similar to that of the input power.

Thus far we have concentrated our attention solely on the driven mode. Figure 23 shows the spectra for dissipated power (those for radiated power are of the same magnitude and opposite sign) in two of the non-driven modes: (3, 7), whose resonance coincides with that of (9, 3), and (11, 3), a mode well coupled to (9, 3). The significant interactions occur at the resonances of (9, 3) and the non-driven mode under consideration, and the effect is clearly more powerful in the resonant/resonant case than in either of the resonant/non-resonant cases, substantiating the assertions of Leppington *et al.* and Mkhitarov. However, the resonant/non-resonant interactions do still affect the overall radiated and dissipated power, biasing the oscillations in figure 21 towards the negative side of the diagonal approximation and appearing as corresponding small peaks in the dissipated power.

We seek explanations for the behaviour seen in figures 20–23 by considering a simplified model, where only two modes interact. This neglects the effect of 'flanking' paths through other modes, but will give a good indication of the behaviour in situations where the interaction between a single mode pair dominates, as appears usually to be the case here. When (2.4) consists simply of two modal equations, for (m, n) and (p, q), the solution is trivial, and

$$Y_{mnmn} = [d_{mn} - (\epsilon_{\mathrm{f0}} Z^{\mathrm{0f}}_{mnpq})^2/d_{pq}]^{-1}, \tag{4.1a}$$

$$Y_{mnpq} = Y_{pqmn} = -(\epsilon_{\mathrm{f0}} Z^{\mathrm{0f}}_{mnpq}/d_{pq})\, Y_{mnmn}. \tag{4.1b}$$

The results for the input power spectrum (figure 20) may now be examined in the light of equation (4.1*a*), taking (m, n) as the driven mode. When (m, n) is at resonance, $d_{mn} \sim \epsilon_{\mathrm{s}}$, and we must consider potential modes (p, q). If (p, q) is also at

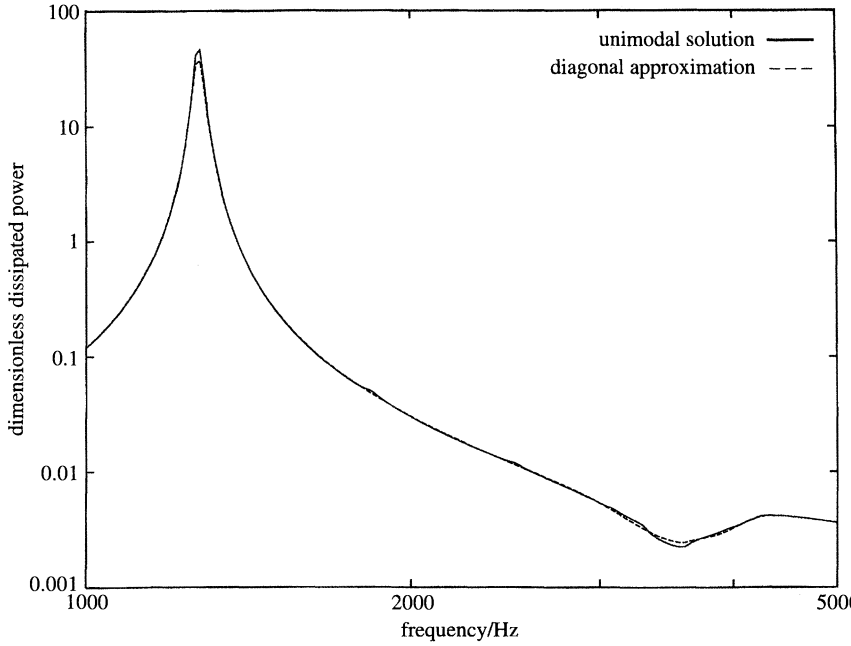

Figure 22. Dimensionless dissipated power spectrum for mode (9, 3): unimodal ($M\omega S^{u}_{dmn}(\omega)/\Phi_c$) and diagonal ($M\omega S^{d}_{dmn}(\omega)/\Phi_c$) solutions. The curves coincide almost exactly away from resonance, explaining the matching input and radiated power behaviour in figures 20 and 21. At resonance, coupling increases the dissipation.

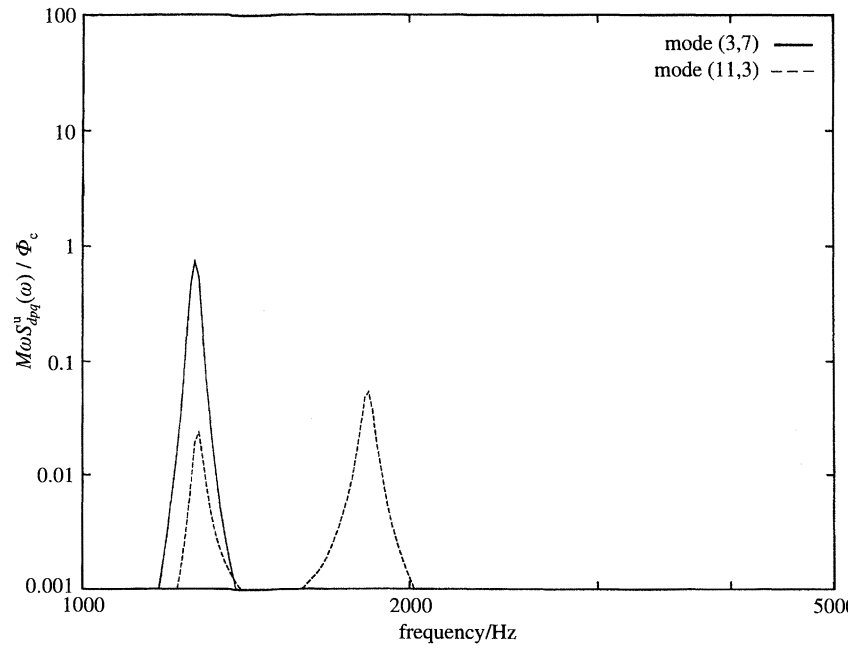

Figure 23. Dimensionless dissipated power spectra for modes (3, 7) and (11, 3): unimodal solution. The dissipation peaks in these non-driven modes arise from two different types of interaction with (9, 3): resonant/resonant for (3, 7) and well coupled, resonant/non-resonant for (11, 3).

resonance, it will not be well coupled to (m,n) (i.e. $m \neq p$ and $n \neq q$), so that $Z^{0f}_{mnpq} \sim O(N^{-2})$. Thus,

$$\frac{(\epsilon_{f0} Z^{0f}_{mnpq})^2}{d_{pq}} \sim \frac{\epsilon_s}{N^2}\left(\frac{\epsilon_{f0}}{N\epsilon_s}\right)^2. \tag{4.2}$$

Alternatively, if (p,q) is not at resonance, then it may be well coupled to (m,n), and $Z^{0f}_{mnpq} \sim O(N^{-1})$, giving

$$(\epsilon_{f0} Z^{0f}_{mnpq})^2/d_{pq} \sim \epsilon_s^2(\epsilon_{f0}/N\epsilon_s)^2, \tag{4.3}$$

assuming $d_{pq} \sim O(1)$. The parameter $N^2\epsilon_s$ varies from 2 to 50 over our frequency range, so that (4.3) represents the more important term, and we must consider the resonant/non-resonant interaction. Since $\epsilon_s^2 \ll \epsilon_s$, and $\epsilon_{f0}/N\epsilon_s \sim O(1)$,

$$\mathrm{Re}\,[Y^*_{mnmn}] \approx \mathrm{Re}\left[\frac{1}{d_{mn}} + \frac{1}{d_{pq}}\left(\frac{\epsilon_{f0} Z^{0f}_{mnpq}}{d_{mn}}\right)^2\right], \tag{4.4}$$

where the difference compared with the diagonal approximation is represented by the second term. In general, Z^{0f}_{mnpq} cannot be simply characterized, but for two well coupled, below coincidence modes the singly-cross case results give $-\frac{1}{2}\pi < \arg(Z^{0f}_{mnpq}) < 0$ almost always. Thus, if (m,n) is at resonance (d_{mn} real) and (p,q) is above resonance ($d_{pq} \sim -\mathrm{i}$), (4.4) implies that the input power will be greater than the diagonal approximation. For (p,q) below resonance, the opposite is true, but most below resonance modes have $|d_{pq}| \gg 1$, so this effect is less significant. We thus expect a net positive bias in the input power when (m,n) is at resonance, as seen in figure 20. On either side of the resonance peak, d^2_{mn} changes rapidly from positive real to negative real, so the sign of the bias reverses, as observed.

Away from resonance, we write

$$\mathrm{Re}\,[Y^*_{mnmn}] = \mathrm{Re}\,[d_{mn} - (\epsilon_{f0} Z^{0f}_{mnpq})^2/d_{pq}]|d_{mn} - (\epsilon_{f0} Z^{0f}_{mnpq})^2/d_{pq}|^{-2}. \tag{4.5}$$

The modulus is dominated by the reactive part of d_{mn}, and is thus essentially the same as $|d_{mn}|^{-2}$. However, since $\mathrm{Re}\,(d_{mn}) \sim \epsilon_s$, the inclusion of coupling may significantly affect the first term, and will do so most effectively if (p,q) is resonant and well coupled to (m,n). Here the condition on $\arg(Z^{0f}_{mnpq})$ implies that the difference from the diagonal approximation will be positive below the (p,q) resonance ($d_{pq} \sim \mathrm{i}$) and negative above ($d_{pq} \sim -\mathrm{i}$), explaining the solitary oscillations seen in figure 20. The sign of the difference at the (p,q) resonance cannot be determined from these arguments; hence the oscillations do not always have zero bias about the diagonal solution. Finally, once (m,n) is efficient, $\mathrm{Re}\,(d_{mn}) \sim \epsilon_{f0}$, so that the effect of interaction with a resonant mode is much smaller. This explains the convergence of the full and diagonal solutions seen in figure 20.

Having considered the input power, it is now necessary to investigate how it is split between radiation and dissipation. The notable feature of the dissipated power in the driven mode is the accuracy of the diagonal solution away from resonance. For unimodal excitation, the dissipation is proportional to

$$|Y_{mnmn}|^2 = |d_{mn} - (\epsilon_{f0} Z^{0f}_{mnpq})^2/d_{pq}|^{-2}, \tag{4.6}$$

and the arguments presented above again hold for the modulus. The modal velocity is thus essentially unchanged from the diagonal approximation except at resonance, where the tendency for input power to increase corresponds to a bias in favour of higher velocity.

The radiated power, equal to the difference between the input and dissipated powers, will therefore reflect the input power characteristics away from resonance, as seen in figure 21. However, the drop at resonance is not so easily explained, because the increase in velocity there must correspond to an increase in acoustic radiation due to the real part of the direct impedance, and the driven mode must therefore be *absorbing* acoustic energy by virtue of the coupling effect. This implies a negative leaky coupling component (which is of the same sign for two interacting modes), in order that the non-driven mode also be absorbing acoustic energy. We therefore conclude that two interacting modes are capable of extracting energy from the ambient acoustic field via the leaky coupling – a highly counter-intuitive concept, because the leaky coupling arises from an integral over radiating wavenumbers. The two-mode model is again useful here, as the interaction terms given in (2.23) may be evaluated exactly in this case. For unimodal excitation, $V_{pqmn} = Y_{pqmn}\, Y^*_{mnmn}\, \Phi_{mnmn}$, so that, writing $Z^{0f}_{mnpq} = \sigma + \mathrm{i}\chi$, $d_{pq} = d_r + \mathrm{i}d_i$ and using (4.1) for Y_{mnmn}, Y_{pqmn}, the direct coupling term becomes

$$-2\epsilon_{f0}\,\mathrm{Im}\,(Z^{0f}_{mnpq})\,\mathrm{Im}\,(V_{pqmn}) = 2\epsilon^2_{f0}[\,\chi^2 d_r - \sigma\chi d_i]\,\Phi_{mnmn}|Y_{mnmn}|^2/|d_{pq}|^2, \quad (4.7a)$$

while the leaky component is given by

$$2\epsilon_{f0}\,\mathrm{Re}\,(Z^{0f}_{mnpq})\,\mathrm{Re}\,(V_{pqmn}) = -2\epsilon^2_{f0}[\sigma^2 d_r + \sigma\chi d_i]\,\Phi_{mnmn}|Y_{mnmn}|^2/|d_{pq}|^2. \quad (4.7b)$$

These equations demonstrate the validity of the arguments presented above. The leaky component is clearly capable of becoming negative, and is certainly so both for (p,q) resonant ($d_i \approx 0$), and for (p,q) mass-limited and well coupled to (m,n) ($\sigma\chi d_i > 0$). Far from counteracting the tendency of the direct coupling terms to increase vibration at the expense of acoustic radiation, the leaky coupling components enhance the effect. Note also that the order of magnitude arguments applied previously show that, although the resonant/non-resonant mode interaction dominates the input power behaviour at the (m,n) resonance, the net energy transfer to mode (p,q) is greatest if it is also resonant, as borne out by figure 23.

Our investigation of the unimodal excitation case is now complete. We have found that, in comparison with the diagonal approximation, the input power tends to rise at the resonance frequency of the driven mode, drop either side of it and then undergo single oscillations at the resonance frequencies of modes well coupled to the driven mode. The dissipated power in the driven mode differs significantly only at resonance, where it has a tendency to increase, whereas the radiated power mirrors the input power behaviour except at resonance, where it is reduced by the negative leaky coupling effect. When the non-driven mode powers are included, the balance is tilted still farther away from radiation, although the additional effect is relatively small. The success of the two-mode model in explaining these phenomena confirms the validity of the assumptions underlying its use.

We may now integrate these observations into an explanation of the behaviour of the mode classes, described in (iii). For any given mode, the input power will simply be the unimodal input power (e.g. figure 20), whereas the radiated and dissipated powers will consist of the unimodal, driven values (e.g. figures 21 and 22) plus a respective decrease and increase due to energy transfer from other modes, now also driven. Thus, for the efficient modes (figure 16), the input power will be close to the diagonal solution, as will the sums of the driven radiation and dissipation. The contribution from other modes will then decrease the radiation and increase the dissipation. However, the efficient modes are extremely difficult to move, being away

PHILOSOPHICAL TRANSACTIONS OF THE ROYAL SOCIETY A MATHEMATICAL, PHYSICAL & ENGINEERING SCIENCES

from resonance and very highly damped (high radiation efficiency), and their structural dissipation is tiny. Thus, although the percentage increase in structural dissipation (and therefore modal velocity) due to this effect is large, the decrease in radiated power is negligible, and it remains close to the diagonal solution.

The mass-limited modes (figure 17) have two potential sources of difference between the full and diagonal solutions for input power. The interactions with resonant modes, however, are small in absolute value and will also tend to cancel in the modal summation (which may crudely be likened to a narrow band frequency average), so that the remaining effect, the negative bias just beyond the resonance peak, will dominate, and the input power will tend to be below the diagonal solution. The radiated and dissipated powers will be similarly determined by values just beyond the resonance peak, where no significant contributions from other driven modes occur, so their behaviour will simply reflect that of the unimodal, driven powers, showing virtually unchanged dissipation and reduced radiation. The characteristics of the resonant modes (figure 18) are also essentially established by the unimodal, driven powers, with input power rising over the diagonal solutions at resonance then dropping either side, radiated power biased lower and dissipated power higher. However, there will also be contributions from other driven modes (when resonances coincide), which will further accentuate the imbalance between radiation and dissipation. Finally, the arguments presented for the mass-limited modes apply equally to the stiffness-limited modes, and they show very similar features (figure 19).

(v) *Requirements for the neglect of coupling*

Having explained the detailed effects of the modal coupling, we may now extract its important aspects and determine when they may be neglected. The characteristics of the overall problem are dominated by the resonant modes, except for the radiated power, where the contribution from efficient modes is also significant. However, this latter feature is essentially unaffected by the coupling, and it is thus the resonant mode behaviour that is relevant. Here, two effects have been found: the resonant/non-resonant interaction with well coupled, mass-limited modes, and the expected interaction with other resonant modes. Coupling may only be neglected if both these effects are small, and appropriate conditions are readily obtained from the two-mode model. If the input power is to follow the diagonal approximation, the correction term in (4.4) must be small, giving

$$N^2\epsilon_s/\epsilon_{f0}^2 \gg 1 \tag{4.8}$$

for the resonant/non-resonant mode interaction, and

$$(N^2\epsilon_s/\epsilon_{f0})^2 \gg 1 \tag{4.9}$$

for the resonant/resonant effect. The situation is less clear for the radiated and dissipated power, but detailed consideration shows that (4.8) and (4.9) apply here too. In our case they are weakly true at 1 kHz, and become increasingly valid at higher frequencies, as borne out by the numerical results.

We may also now consider the situation where there is not significant overlapping of resonant modes. In this case, the only relevant interaction is that between resonant and non-resonant, well coupled modes, so (4.8) is the sole requirement. This condition, though, was derived assuming $\mathrm{Re}\,(d_{mn}) \sim \epsilon_s$, which is true for most below coincidence modes if (4.9) is satisfied. If not, we shall typically have

$\mathrm{Re}\,(d_{mn}) \sim \epsilon_{\mathrm{f}0}/N^2$, and (4.8) then becomes $\epsilon_{\mathrm{f}0} \ll 1$. When resonances are distinct, coupling may be neglected *however small the structural damping* if the fluid-loading is light, and otherwise condition (4.8) only is required.

These conditions for the neglect of coupling below the critical frequency are still more restrictive than the simple $N \gg 1$ requirement above it (Leppington *et al.* 1986). However, they are not stringent, and this raises the possibility of applying the SEA approach to situations with signiicant fluid-loading. To assess this idea, we now present a modified SEA analysis and its results for the flat-plate problem considered here.

(c) *Application of SEA to the fluid-loaded plate*

(i) *Analysis*

The problem of applying SEA to a fluid-loaded plate radiating to infinity has been considered by a number of authors, including Heron (1977), Davies (1971*a*) and Leppington *et al.* (1986). However, all these analyses have applied to light fluid-loading situations, and require modification in this case. We shall demonstrate how this may be achieved, using the approach of Leppington *et al.* as a basis for investigation.

The SEA analysis starts with the diagonal approximation for the radiated power spectrum, and considers frequency-averaged values. From (2.13) and (2.19), the dimensionless frequency-averaged spectrum may be written as

$$\frac{M\omega_0}{\Phi_{\mathrm{c}}}\langle S_0^{\mathrm{d}}(\omega_0)\rangle = \frac{2\rho_0 c_0 \omega_0}{M\,\Delta\omega} \sum_{m,n} \int_{\omega_0-\frac{1}{2}\Delta\omega}^{\omega_0+\frac{1}{2}\Delta\omega} \frac{\sigma_{mn}(\omega)}{\omega^2|d_{mn}|^2}\,\mathrm{d}\omega, \tag{4.10}$$

where $\sigma_{mn}(\omega) = \mathrm{Re}\,(Z^{0\mathrm{f}}_{mnmn})$, and it is assumed that $\Delta\omega/\omega_0 \ll 1$, but also that the frequency band is sufficiently wide to include several resonant modes. The significant contributions to $\langle S_0^{\mathrm{d}}(\omega_0)\rangle$ come from the resonant (class 3) and efficient (class 1) modes, so we write $\langle S_0^{\mathrm{d}}(\omega_0)\rangle = \langle S_0^{\mathrm{d}}(\omega_0)\rangle_{\mathrm{res}} + \langle S_0^{\mathrm{d}}(\omega_0)\rangle_{\mathrm{eff}}$ and treat each component separately.

The first, $\langle S_0^{\mathrm{d}}(\omega_0)\rangle_{\mathrm{res}}$, is found by noting that, for a resonant mode (m,n), the behaviour of the integrand is dominated by the rapidly varying term $|d_{mn}|^{-2}$. When fluid-loading is light, $\mathrm{Im}\,(Z^{0\mathrm{f}}_{mnmn})$ may be neglected in d_{mn} (equation (2.10)) and Leppington *et al.* obtain, in our notation,

$$(M\omega_0/\Phi_{\mathrm{c}})\langle S_0^{\mathrm{d}}(\omega_0)\rangle_{\mathrm{res}} \approx \pi\omega_0 n_{\mathrm{s}} \epsilon_{\mathrm{f}0}\langle\sigma(N_{\mathrm{p}})\rangle/\langle\epsilon\rangle \tag{4.11}$$

where n_{s} is the plate modal density,

$$n_{\mathrm{s}} = (ab/4\pi)(M/B_{\mathrm{r}})^{\frac{1}{2}}, \tag{4.12}$$

$\langle\sigma(K_{mn})\rangle$ the mean radiation efficiency for a dimensionless modal wavenumber K_{mn} $(= k_{mn}/k_0)$, $\langle\epsilon\rangle$ the mean modal damping, $\epsilon_{\mathrm{s}} + \epsilon_{\mathrm{f}0}\langle\sigma\rangle$, and N_{p} the dimensionless plate wavenumber. Implicit in this solution is the assumption that $\langle\sigma_{mn}/(\epsilon_{\mathrm{s}} + \epsilon_{\mathrm{f}0}\sigma_{mn})\rangle = \langle\sigma\rangle/\langle\epsilon\rangle$, which is only certainly true when $\epsilon_{\mathrm{f}0}\sigma_{mn} \ll \epsilon_{\mathrm{s}}$, or $\gg \epsilon_{\mathrm{s}}$. With this caveat, the solution is completed by the expression of Leppington *et al.* for $\langle\sigma\rangle$, found by approximating the summation with an integral:

$$\langle\sigma(K_{mn})\rangle = \frac{\mu+\eta}{\pi K_{mn}\mu\eta(K_{mn}^2-1)^{\frac{1}{2}}}\left[\ln\left(\frac{K_{mn}+1}{K_{mn}-1}\right) + \frac{2K_{mn}}{K_{mn}^2-1}\right]. \tag{4.13}$$

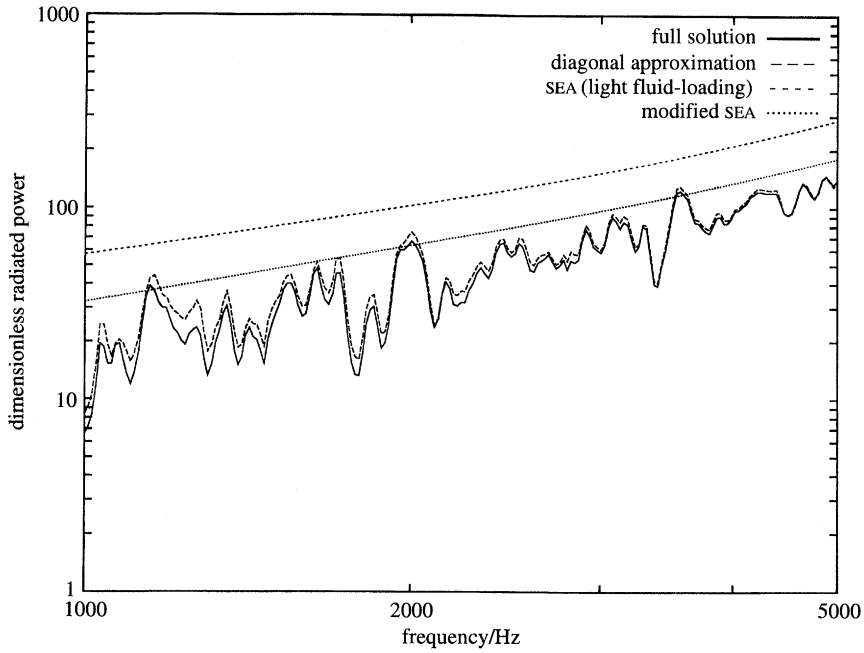

Figure 24. Class 3 modes: comparison of full ($M\omega S_0(\omega)/\Phi_c$), diagonal ($M\omega S_0^d(\omega)/\Phi_c$) and SEA ($M\omega\langle S_0(\omega_0)\rangle/\Phi_c$) solutions for the radiated power. The light fluid-loading SEA result takes no account of added mass due to the fluid and overestimates significantly compared with the modified formula.

For heavier fluid-loading, the effect of the added mass due to the imaginary part of Z^{0f}_{mnmn} is significant, and d_{mn} is now given by

$$d_{mn} \approx \mathrm{i}\left[\frac{k_{mn}^4}{n_p^4} - \tilde{m}\right] + \left[\frac{k_{mn}^4}{n_p^4}\epsilon_s + \epsilon_{f0}\,\sigma_{mn}\right], \tag{4.14}$$

with

$$\tilde{m} = 1 + \epsilon_{f0}/(K_m^2 + K_n^2 - 1)^{\frac{1}{2}}. \tag{4.15}$$

For the resonant modes, where $K_m^2 + K_n^2$ is specified by the condition $K_{mn} = \tilde{m}^{\frac{1}{4}}N_p$, $\tilde{m}$ is a slowly varying function of ω_0, and using this fact a similar analysis to that of Leppington *et al.* may be followed, with result

$$(M\omega_0/\Phi_c)\langle S_0^d(\omega_0)\rangle_{res} \approx \frac{\pi\omega_0\, n_s'\,\epsilon_{f0}\langle\sigma(\tilde{m}^{\frac{1}{4}}N_p)\rangle}{\tilde{m}^2\langle\epsilon'\rangle}, \tag{4.16}$$

where $n_s' = \tilde{m}^{\frac{1}{2}}n_s$ and $\langle\epsilon'\rangle = \epsilon_s + \epsilon_{f0}\langle\sigma\rangle/\tilde{m}$. The resonance condition only specifies K_{mn} implicitly, but a satisfactory approximation is obtained after the first step of an iterative solution starting with $K_{mn} = N_p$.

The non-resonant term, $\langle S_0^d(\omega_0)\rangle_{eff}$, arising as it does from the slowly-varying, efficient modes, is evaluated by neglecting the frequency average (corresponding to an assumption of constant integrand over the frequency range considered) and approximating the sum by an integral in wavenumber space. Again following Leppington *et al.*, we obtain

$$\frac{M\omega_0}{\Phi_c}\langle S_0^d(\omega_0)\rangle_{eff} \approx \frac{\epsilon_{f0}\,\mu\eta}{\pi}\int_0^1 \frac{K_{mn}(1-K_{mn}^2)^{-\frac{1}{2}}}{|d_{mn}|^2}\,\mathrm{d}K_{mn}. \tag{4.17}$$

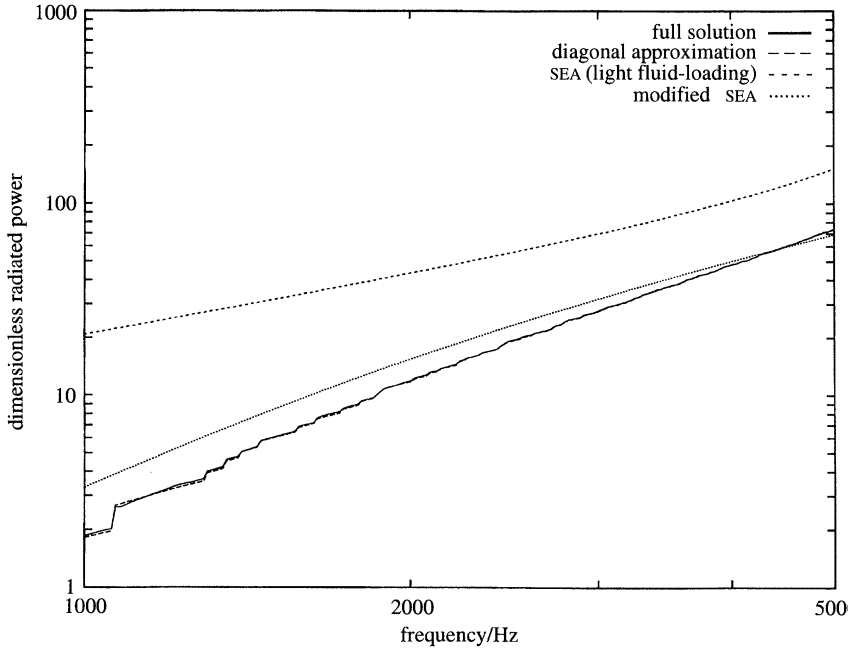

Figure 25. Class 1 modes: comparison of full ($M\omega S_0(\omega)/\Phi_c$), diagonal ($M\omega S_0^d(\omega)/\Phi_c$) and SEA ($M\omega_0\langle S_0^d(\omega_0)\rangle/\Phi_c$) solutions for the radiated power. Here, inclusion of the effect of radiation damping on the response, neglected in the light fluid-loading SEA formula, significantly improves the prediction.

For light fluid-loading, d_{mn} is dominated by the reactive term $\mathrm{i}(K_{mn}^4/N_p^4-1)$ and the result is the approximation of Leppington *et al.*:

$$\frac{M\omega_0}{\Phi_c}\langle S_0^d(\omega_0)\rangle_{\mathrm{eff}} \approx \frac{\epsilon_{f0}\mu\eta}{4\pi}\left[\frac{N_p^4}{N_p^4-1}+\tfrac{1}{2}N_p^2\left\{\frac{3N_p^2+2}{(N_p^2+1)^{\frac{3}{2}}}\operatorname{artanh}\left[(N_p^2+1)^{-\frac{1}{2}}\right]+\frac{3N_p^2-2}{(N_p^2-1)^{\frac{3}{2}}}\arctan\left[(N_p^2-1)^{-\frac{1}{2}}\right]\right\}\right]. \quad (4.18)$$

For heavier fluid-loading, however, the radiation damping in d_{mn} is significant and a more appropriate form is therefore

$$d_{mn} \approx -\mathrm{i}+\epsilon_{f0}[1-K_{mn}^2]^{-\frac{1}{2}}, \quad (4.19)$$

in which case (4.17) becomes

$$(M\omega_0/\Phi_c)\langle S_0^d(\omega_0)\rangle_{\mathrm{eff}} \approx (\epsilon_{f0}\mu\eta/\pi)[1-\epsilon_{f0}\arctan(\epsilon_{f0}^{-1})]. \quad (4.20)$$

Equations (4.20) and (4.18) match for cases with light fluid-loading and purely mass-limited efficient modes ($\epsilon_{f0} \ll 1, N_p \gg 1$), as would be expected.

(ii) *Comparison with modal results*

Figures 24–26 show the comparisons between modal evaluations of $S_0(\omega)$ and the SEA approximations. In each case, both full and diagonal solutions are plotted, along with the light fluid-loading and modified SEA expressions. For the resonant modes (figure 24), the neglect of added mass in the formulae of Leppington *et al.* leads to a result that is significantly too high, whereas the heavy fluid-loading expression is

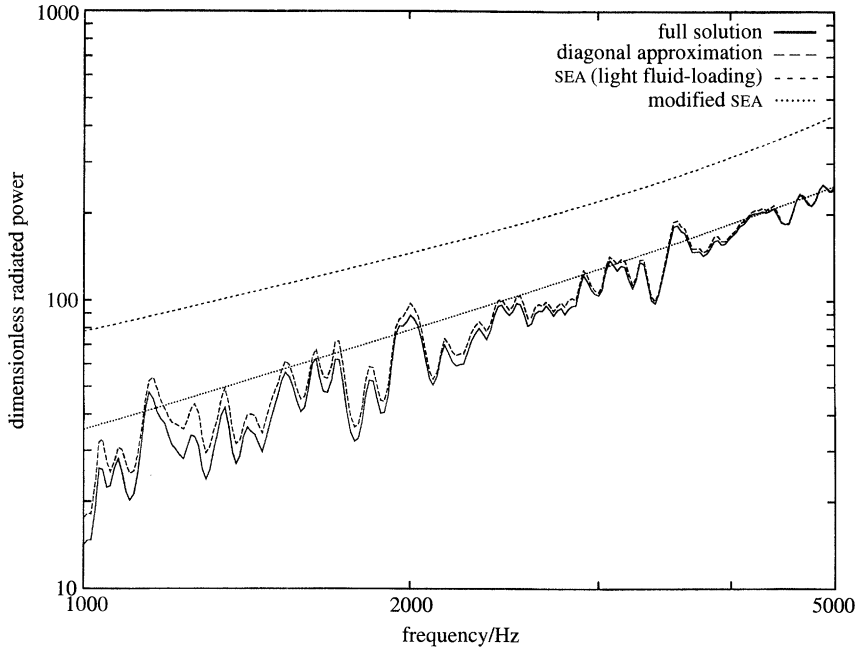

Figure 26. Comparison of full ($M\omega S_0(\omega)/\Phi_c$), diagonal ($M\omega S_0^d(\omega)/\Phi_c$) and SEA ($M\omega\langle S_0^d(\omega_0)\rangle/\Phi_c$) solutions for the overall radiated power. The pattern of figures 24 and 25 is repeated, except that the agreement between the modal solutions and modified SEA is better, owing to the contributions of class 2 and 4 modes to the overall radiation.

only slightly above the average value of the diagonal solution. A similar trend is seen for the efficient modes (figure 25), the high radiation damping being crucial in this problem. As a result, the overall solutions (figure 26) show the same behaviour as the two components, with the exception that the modified SEA approximation is now more accurate. This is due to the relatively small, but not insignificant, contributions from class 2 and class 4 modes, which raise the modal solutions.

So, as expected, the light fluid-loading expressions are not successful in predicting the power radiated by a significantly fluid-loaded plate. However, the approach used to derive them is easily modified to suit the different parameter régime, and the new expressions provide reasonably accurate predictions, given the approximations inherent in the SEA approach.

5. Conclusions

The work presented in this paper has investigated the validity of two common approximations in the analysis of the vibration and radiation of fluid-loaded plates, namely the neglect of modal coupling (the diagonal approximation) and the SEA approach. The asymptotic evaluation of the modal coupling terms, presented in §3, makes numerical solution of the fully coupled modal equations feasible, and it has thus been possible to compare the results of the two approximate approaches with the full solution for a practical problem, and thereby to gain an appreciation of their applicability.

The comparison between the coupled and diagonal solutions demonstrates the complicated nature of modal coupling due to an acoustic field. Contrary to previous

assumptions, the coupling does not act solely to transfer energy from one mode to another (direct coupling), but also results in an interaction between the two modes and the ambient acoustic field that is of the same sign for each mode (leaky coupling). It is therefore hard to find simple arguments that explain its effect, but a model assuming interaction between two modes only has been successful in providing a qualitative interpretation of the phenomena observed in the full solution. In comparison with the diagonal approximation, these are essentially an unbiased fluctuation in input power from the driving forces, and a bias in favour of increased vibration (structural dissipation) at the expense of acoustic radiation. Again contradicting previous assumptions, these effects have been found to arise not only from the interaction of resonant modes, but also from resonant/non-resonant interactions. As a result of this improved understanding, new conditions for the neglect of modal coupling have been obtained ((4.8) and (4.9)).

The comparison with SEA results shows that existing expressions, valid for light fluid-loading, are inaccurate in the significantly fluid-loaded problem considered here. However, the SEA approach may still be applied, with appropriate modifications, and has been found to yield formulae that are useful and accurate, particularly at high frequencies.

When considering the applicability of the approximate methods to engineering problems, it is necessary to discuss the generality of the conditions derived here. These are valid for a simply supported plate, undergoing forcing that does not couple the modes. However, Lomas & Hayek (1977) have shown how the vibration of a plate with arbitrary edge conditions may be expressed in terms of the simply supported formulation, by writing the true modes as weighted sums of the simply supported mode functions. This may affect the condition for negligible resonant/resonant mode interaction (equation (4.9), where it is assumed the modes are poorly coupled), but, as the sum for a given mode will usually be dominated by the nearest corresponding simply supported mode, the difference should not be great. The effect of coupled forcing is small either if the cross-modal excitation term Φ_{rsij} is small, or if the cross-modal impedance is small, and for high frequencies they are both typically $O(N^{-2})$. This complication should therefore also not alter the conditions presented here greatly, and they may thus be assumed to have a generality beyond the simple case investigated.

We conclude, then, that for most load-bearing engineering structures surrounded by unbounded fluid, the diagonal approximation will be sufficiently accurate, except possibly at low frequencies. SEA approximations may also be useful, but the assumptions involved in their derivation may require tailoring to suit individual situations.

The work presented in this paper was undertaken with financial support from British Aerospace (Regional Aircraft) Limited. The author is also indebted to his supervisor, Dr Ann Dowling, whose advice and encouragement have been invaluable.

References

Abramowitz, M. & Stegun, I. A. 1965 *Handbook of mathematical functions*. New York: Dover Publications.

Bano, S., Marmey, R., Jourdan, L. & Guibergia, J.-P. 1992 Étude théorique et expérimentale de la réponse vibro-acoustique d'une plaque couplée à une cavité en fluide lourd. *J. acoust.* **5**, 99–124.

Blake, W. K. 1986 Essentials of turbulent wall-pressure fluctuations. Chapter 8 of *Mechanics of flow-induced sound and vibration*, vol. II (*Complex flow-structure interactions*). New York and London: Academic Press.

Chang, Y. M. & Leehey, P. 1979 Acoustic impedance of rectangular panels. *J. Sound Vib.* **64**, 243–256.

Davies, H. G. 1971*a* Sound from turbulent-boundary-layer-excited panels. *J. acoust. Soc. Am.* **49**, 878–889.

Davies, H. G. 1971*b* Low frequency random excitation of water-loaded rectangular plates. *J. Sound Vib.* **15**, 107–126.

Graham, W. R. 1993 Boundary-layer noise and vibration. Ph.D. thesis, Cambridge University, U.K.

Heron, K. H. 1977 Boundary-layer-induced cabin noise. Ph.D. thesis, Institute of Sound and Vibration Research, University of Southampton, U.K.

Hwang, Y. F. & Maidanik, G. 1990 A wavenumber analysis of the coupling of a structural mode and flow turbulence. *J. Sound Vib.* **142**, 135–152.

Keltie, R. F. & Peng, H. 1987 The effects of modal coupling on the acoustic power radiation from panels. *Trans. Am. Soc. mech. Engrs: J. Vibr., Acoust., Stress Reliab. Des.* **109**, 48–54.

Leppington, F. G., Broadbent, E. G. & Heron, K. H. 1982 The acoustic radiation efficiency of rectangular panels. *Proc. R. Soc. Lond.* A **382**, 245–271.

Leppington, F. G., Broadbent, E. G., Heron, K. H. & Mead, S. M. 1986 Resonant and non-resonant acoustic properties of elastic panels. I. The radiation problem. *Proc. R. Soc. Lond.* A **406**, 139–171.

Lomas, N. S. & Hayek, S. I. 1977 Vibration and acoustic radiation of elastically supported rectangular plates. *J. Sound Vib.* **52**, 1–25.

Mkhitarov, R. A. 1972 Interaction of the vibrational modes of a thin bounded plate in a liquid. *Soviet Phys. Acoust.* **18**, 123–126.

Pope, L. D. & Leibowitz, R. C. 1974 Intermodal coupling coefficients for a fluid-loaded rectangular plate. *J. acoust. Soc. Am.* **56**, 408–415.

Press, W. H., Flannery, B. P., Teukolsky, S. A. & Vetterling, W. T. 1989 Solution of linear algebraic equations. Chapter 2 of *Numerical recipes*. Cambridge University Press.

Sandman, B. E. 1975 Motion of a three-layered elastic-viscoelastic plate under fluid loading. *J. acoust. Soc. Am.* **57**, 1097–1107.

Received 7 January 1993; accepted 20 April 1994

PHILOSOPHICAL TRANSACTIONS OF THE ROYAL SOCIETY A MATHEMATICAL, PHYSICAL & ENGINEERING SCIENCES